NACA RM L57A09

NACA

# RESEARCH MEMORANDUM

## MEASUREMENT OF STATIC PRESSURE ON AIRCRAFT

By William Gracey

Langley Aeronautical Laboratory
Langley Field, Va.

NATIONAL ADVISORY COMMITTEE
FOR AERONAUTICS

WASHINGTON

April 1, 1957
Declassified April 15, 1958

TABLE OF CONTENTS

NACA RM L57A09

NATIONAL ADVISORY COMMITTEE FOR AERONAUTICS

---

RESEARCH MEMORANDUM

---

# MEASUREMENT OF STATIC PRESSURE ON AIRCRAFT

By William Gracey

## SUMMARY

Existing data on the errors involved in the measurement of static pressure by means of static-pressure tubes and fuselage vents are presented. The errors associated with the various design features of static-pressure tubes are discussed for the condition of zero angle of attack and for the case where the tube is inclined to the flow. Errors due to variations in the configuration of static-pressure vents are also presented. Errors due to the position of a static-pressure tube in the flow field of the airplane are given for locations ahead of the fuselage nose, ahead of the wing tip, and ahead of the vertical tail fin. The errors of static-pressure vents on the fuselage of an airplane are also presented.

A comparison of the calibrations of the four static-pressure-measuring installations indicates that, for an airplane designed to operate at supersonic speeds, a static-pressure tube located ahead of the fuselage nose will, in general, be the most desirable installation. If the operating range is confined to speeds below sonic, a static-pressure tube located ahead of the wing tip may, for some airplane configurations, prove more satisfactory than a fuselage-nose installation. For operation at Mach numbers below 0.8, a static-pressure tube ahead of the vertical tail fin or fuselage vents, properly located and installed, should prove satisfactory.

Various methods of calibrating static-pressure installations in flight are briefly discussed.

## INTRODUCTION

The proper functioning of fire-control and guidance systems for airplanes and missiles depends fundamentally on the accurate measurement of total and static pressures. For each of these measurements the basic problem is that of determining what type of sensing device to use and where to locate it on the flight vehicle.

The National Advisory Committee for Aeronautics has been studying this problem for many years. A comprehensive survey of the subject, based on information obtained at subsonic speeds, was published in 1948 (ref. 1). Since that time additional data have been obtained from wind-tunnel, rocket-model, and flight tests in the transonic and low supersonic speed ranges. Because of current interest in this information, it appeared appropriate at this time to present these data and to review the overall problem in the light of this new knowledge.

The measurement of total pressure is not discussed in this paper because this measurement can be accomplished quite accurately with little or no difficulty, and because the subject has been adequately treated in other reports. The problems involved in the design and location of a total-pressure tube on the airplane are discussed in reference 1. The only error of any consequence in the measurement of total pressure is that due to the inclination of the tube to the airstream. This error can be avoided by using a swiveling tube or a suitably designed rigid tube. Information required for designing a rigid tube which will measure total pressure correctly over a wide range of angle of attack at both subsonic and supersonic speeds may be found in reference 2.

## SYMBOLS

| | |
|---|---|
| $p$ | free-stream static pressure |
| $p'$ | indicated static pressure |
| $\Delta p$ | static-pressure error, $p' - p$ |
| $p_t$ | total pressure |
| $q$ | dynamic pressure, $\frac{1}{2}\rho V^2$ |
| $q_c$ | impact pressure, $p_t - p$ |
| $M$ | free-stream Mach number |
| $M'$ | measured Mach number |
| $T$ | ambient temperature, absolute units |
| $T'$ | measured temperature, absolute units |
| $K$ | temperature recovery factor, $\frac{T' - T}{0.2M^2T}$ |

| | |
|---|---|
| $\rho$ | mass density of air |
| R | gas constant (53.3) |
| $N_{Re}$ | Reynolds number |
| r | radius of curvature |
| $C_L$ | lift coefficient |
| $C_N$ | normal-force coefficient |
| h | altitude |
| d | diameter of static-pressure tube; diameter of orifice |
| D | diameter of collar on static-pressure tube; maximum diameter of model or fuselage |
| t | maximum thickness of stem on static-pressure tube; maximum thickness of wing or vertical tail fin |
| $l$ | length of model |
| $l'$ | twice distance from nose of model to maximum-diameter station |
| x | axial position of static-pressure orifice from reference point |
| y | height of protuberance near static-pressure orifice |
| $\alpha$ | angle of attack |
| $\varphi$ | circumferential position of static-pressure orifices |
| $\gamma$ | ratio of specific heats (1.4 for air) |

Subscripts:

| | |
|---|---|
| 1 | lower limit |
| 2 | upper limit |

## STATIC-PRESSURE MEASUREMENT

The sensing device which has been universally used for the measurement of static pressure is a surface orifice oriented parallel to the flight path. Orifices are installed either in the walls of the body of the aircraft or on a tube attached to some part of the aircraft. In either case the pressure at the point in the airstream where the orifice is located usually differs from the free-stream value because the air flowing over the aircraft creates a flow field in which the pressures vary widely from one point to another. At subsonic speeds the flow field extends in all directions for a considerable distance from the aircraft. At supersonic speeds the field is confined to the regions behind the shock waves which form ahead of the aircraft.

The amount by which the local static pressure at a given point in the flow field differs from free-stream static pressure is called the "position error" of the installation. If the static-pressure source is a static-pressure tube, there may be an additional error due to the flow field created by the tube. The flow field around the aircraft as well as that around the tube changes primarily with Mach number and angle of attack, and secondarily with Reynolds number. The pressure developed at the static-pressure orifice is, therefore, a function of these variables.

The most difficult problem in designing a static-pressure installation is that of locating the static-pressure source (tube or vent) on the aircraft, because the flow field of each aircraft configuration is unique. Because of the impossibility of finding a location on or close to the aircraft where the static-pressure error is zero for all flight conditions, the problem becomes one of choosing a location where the error is of sufficiently small magnitude or where it varies uniformly with Mach number and angle of attack. Generally, the greater the distance from the aircraft that the static-pressure source can be located (preferably ahead of the aircraft), the more nearly will this objective be realized. For such remote locations of the static-pressure source, the magnitude and variation of the static-pressure error can be predicted with some success from the calibrations of similar installations on other aircraft.

The actual errors of a given installation, however, can be determined only by a calibration in flight. Such a flight calibration establishes the overall static-pressure error, that is, the error due to the location of the static-pressure source and the error due to the source itself. If the resulting errors are higher than desired, corrections may be applied either before or after the pressure indication is displayed. Even when corrections can be applied, however, it is advisable to choose an installation with as small an error as practical because,

in general, the greater the magnitude of the corrections the more they will change with each change in flight condition and the more inaccurate and involved will be the calibration and correction procedure.

Inaccuracies in static-pressure measurement may also arise from instrument errors and from errors due to pressure lag of the tubing that connects the instrument to the static-pressure source. A general discussion of instrument and pressure-lag errors may be found in reference 1. Other aspects of the pressure-lag problem are treated in references 3 and 4.

## STATIC-PRESSURE ERRORS OF TUBES

The flow field around an isolated static-pressure tube is determined by the shape of the nose section, the size and shape of any protuberance on the rear portion of the tube, the Mach number, the angle of attack, and the Reynolds number.

### Tubes at Zero Angle of Attack

For the condition of zero angle of attack, the pressure registered by a static-pressure tube at a given Mach number depends on the axial location of the orifices along the tube and the size and configuration of the orifices.

Axial location of orifices rearward of the nose.- The variation of static pressure along a static-pressure tube may be illustrated by two examples of theoretical pressure distributions over the forward portions of tubes at zero angle of attack. Figure 1 presents a subsonic (incompressible flow) pressure distribution for a tube with a parabolic nose (ref. 5) and a typical supersonic pressure distribution for a tube with a conical nose.

The symbol $\Delta p$ in this figure denotes the static-pressure error, which is defined by the relation $\Delta p = p' - p$, where $p'$ is the static pressure measured by the tube and $p$ is free-stream static pressure. For the theoretical case considered in figure 1, $\Delta p$ is expressed as a fraction of the dynamic pressure $q$; for most of the experimental data presented subsequently, $\Delta p$ is expressed as a fraction of the impact pressure $q_c$. With a few exceptions, the values of $\Delta p/q$ and $\Delta p/q_c$ are in all cases plotted to the same scale.

The two curves in figure 1 show that, downstream from the end of the nose sections, the pressures at subsonic and supersonic speeds are below free-stream static pressure. With increasing distance from the

nose, the pressures in both speed ranges approach the free-stream value. At supersonic speeds, however, the return to free-stream pressure occurs farther downstream. The axial location of orifices on a tube designed to function at both subsonic and supersonic speeds would, therefore, be determined by the pressure distribution at supersonic speeds.

Experimental data showing the variation of static-pressure error with axial location of orifices on three tubes are presented in figure 2. The subsonic data were obtained with a tube with a truncated ogival nose (ref. 6), whereas the supersonic data were determined with tubes having a more elongated truncated ogival nose (ref. 7) and a conical nose (ref. 8). Note that the axial locations of the orifices on these tubes are referenced to the end of the nose section rather than the tip of the nose as in figure 1. The data from investigations conducted with these tubes show that at subsonic speeds ($M = 0.6$ to $0.9$) a static-pressure error of 1/2 percent of $q_c$ is reached at a distance of 4 tube diameters behind the end of the nose section. At supersonic speeds ($M = 1.55$ to $2.87$) an error of 1/2 percent of $q_c$ is reached at 5 to 7 diameters rearward of the nose section.

The effect of varying the shape of the nose of a static-pressure tube has also been determined at both subsonic and supersonic speeds. Subsonic tests ($M = 0.3$ to $0.95$) of tubes having hemispherical, ogival, and truncated ogival noses showed that, when the orifices were located 6 or more tube diameters behind the end of the nose section, the static-pressure errors of the three tubes were in close agreement (ref. 6). Supersonic tests ($M = 1.61$) of tubes having cylindrical, hemispherical, $30^\circ$ conical, short ogival, and long ogival noses showed that, for orifice locations at least 10 diameters rearward of the nose section, the measured pressures were substantially independent of the shape of the nose (ref. 9).

From all of these results, it may be concluded that a tube with orifices located 10 or more diameters behind the end of the nose section will measure free-stream static pressure with small error at both subsonic and supersonic speeds, and that for this axial location of the orifices the measured pressure will be unaffected by the shape of the nose.

The investigations referred to in the previous paragraphs were conducted with small-scale tubes in small-throated tunnels. Tests of a larger (0.97-inch-diameter) tube in the Langley 8-foot transonic tunnel provide full-scale confirmation of this work at subsonic speeds. This tube had a truncated ogival nose with orifices located 7.8 diameters rearward of the end of the nose section. The calibration of this tube (fig. 3) shows the static-pressure error to be within $\pm 1/2$ percent of $q_c$ up to $M = 0.95$.

Axial location of orifices ahead of protuberances.- The pressure developed by a static-pressure tube depends not only on the axial location of the orifices behind the nose but also on the location ahead of protuberances on the rear of the tube. Protuberances may be either transverse stems or collars (expansion of tube to accommodate a support or boom of larger diameter than tube).

The effect of a transverse stem may be seen from figure 4, which presents the theoretical pressure distribution (incompressible flow) ahead of a body of infinite span (ref. 5). The static-pressure errors shown by this curve would apply to a tube with a stem extending from two sides; for a stem extending from only one side, the values would be halved. It will be seen from figure 4 that the static-pressure error due to the stem ("blocking effect") is positive, and decreases rapidly with increasing distance from the stem.

Experimental effects at subsonic speeds of a streamlined stem extending on one side of a tube (ref. 6) are given in figure 5. These data show that the static-pressure error decreases with distance ahead of the stem and increases, at high subsonic speeds, with Mach number. For orifices located a distance of about 10 times the stem thickness ahead of the stem, the static-pressure error will be within 1/2 percent of $q_c$ for Mach numbers up to 0.7. The fact that the error caused by protuberances is positive is often used in the design of a static-pressure tube to compensate for the negative error due to the pressure distribution along the forward portion of the tube.

Data from reference 6 on the blocking effect of collars at subsonic speeds are presented in figure 6. In these tests the ratio of collar diameter to tube diameter was fixed and the position of the collar with respect to the orifices was varied. The distance of the orifices from the nose section (12 tube diameters) was such that the error of the tube without the collar was essentially zero. The results indicate that the static-pressure error decreases with distance of the collar from the orifices and that, for $x/D$ greater than 3.2, the variation of static-pressure error with Mach number is negligible up to $M = 0.95$ with $\alpha = 0^\circ$. The data shown in this figure apply to a ratio of collar to tube diameter $D/d$ of 1.43; for larger values of $D/d$, the blocking effect of the collar will be greater.

The calibration of a 0.91-inch-diameter tube with a collar behind the orifices and $\alpha = 0^\circ$ is given in figure 7. These data, obtained from tests in the Langley 8-foot transonic tunnel, show the static-pressure error to be about +1/2 percent of $q_c$ up to $M = 0.9$. Tests of similar tubes in other wind tunnels (refs. 10 and 11) showed the errors below $M = 0.9$ to be as high as 2 percent of $q_c$.

## Tubes at Angles of Attack

The pressure developed by a static-pressure tube at an angle of attack other than $0^\circ$ depends not only on the axial location of the orifices but also on their circumferential positions. When orifices encircle the tube, the measured static pressure decreases with inclination of the tube, and the variation of static-pressure error with inclination is the same for angles of attack and angles of yaw. The static-pressure error of a tube with this orifice configuration remains within 1 percent of $q_c$ of the value at $\alpha = 0^\circ$ over an angular range of about $\pm 5^\circ$ (ref. 12). The additional error resulting from the inclination of the tube can be avoided by pivoting the tube so that it always alines itself with the airstream. Because of the relative fragility of swiveling tubes, however, attempts have been made to devise rigid tubes which would remain insensitive over an appreciable range of angle of attack.

The basis of these attempts is the pressure distribution around a cylinder. Figure 8 presents the results of pressure-distribution tests of a 2-inch-diameter cylinder at angles of attack of $30^\circ$ and $45^\circ$ and at low subsonic speeds ($M < 0.2$). These curves show the static-pressure error to be positive on the bottom of the cylinder, negative on the top, and zero at a circumferential position of about $30^\circ$ from the bottom. It would appear, therefore, that insensitivity to inclination might be accomplished either by locating orifices at a circumferential position of about $\pm 30^\circ$ or by placing orifices along the top and bottom of the tube to achieve compensation of the positive and negative pressures. The application of both of these methods will be discussed.

The data from reference 13, as exemplified in figure 8, show that, at low subsonic speeds and at $\alpha > 30^\circ$, the pressure distribution at circumferential positions greater than $30^\circ$ varies appreciably with the Reynolds number. In another investigation (ref. 14) in which cylinders at $\alpha = 90^\circ$ were tested at higher Mach numbers (0.3 to 2.9), the effect of Reynolds number on the pressure distribution was found to be negligible at supersonic speeds.

Orifices at $\pm 30^\circ$ location.- The effect of angle of attack at subsonic speeds for a 1-inch-diameter tube with orifices located on the bottom of the tube $30^\circ$ on either side of a vertical radius is reported in reference 15. Sample results of these tests (fig. 9) show that the static-pressure error remains within 1 percent of $q_c$ of the value at $\alpha = 0^\circ$ for angles of attack up to at least $20^\circ$ at $M = 0.30$ and to $9^\circ$ at $M = 0.65$. At angles of yaw the angle-of-attack range for an error of 1 percent of $q_c$ is about $\pm 5^\circ$ (ref. 15).

Supersonic tests of a 0.05-inch-diameter probe with orifices at a circumferential position of $\pm 33^\circ$ are reported in reference 8. The calibrations of this tube (fig. 10) show that the static-pressure error remains within 1 percent of $q_c$ for angles of attack up to $17^\circ$ at $M = 1.56$ and up to at least $8^\circ$ at $M = 2.92$.

Supersonic tests of a 0.63-inch-diameter tube with orifices at a circumferential position of $\pm 37.5^\circ$ are reported in reference 16. The results of these tests (fig. 11) show the static-pressure error to remain within 1 percent of $q_c$ for angles of attack up to at least $12^\circ$ at $M = 1.57$ and at least $15^\circ$ at $M = 1.88$.

Orifices on top and bottom of tube.- Calibrations at angles of attack of a 0.91-inch-diameter tube with four orifices on the top of the tube and seven on the bottom were determined at several Mach numbers between 0.20 and 0.68 (ref. 17). Data for these two Mach numbers (fig. 12) show that the static-pressure error remains within 1 percent of $q_c$ of the value at $\alpha = 0^\circ$ for angles of attack up to $40^\circ$ at $M = 0.20$ and to $18^\circ$ at $M = 0.68$. At some angle of attack above $30^\circ$ and at M above 0.3 the static pressure registered by the tube increases abruptly and fluctuates erratically. For angles of attack between $15^\circ$ and $30^\circ$ and Mach numbers between 0.2 and 0.68 the static-pressure error was found to increase as much as 2 percent of $q_c$ for a change in Reynolds number (based on the local velocity and the diameter of the tube) of from 100,000 to 250,000. Because of the unsymmetric arrangement of the orifices, the sensitivity of the tube at angles of yaw is, like that of the $\pm 30^\circ$ orifice arrangement, much greater than at angles of attack. At angles of yaw the error remained within 1 percent of $q_c$ over an angular range of $\pm 5^\circ$ at $M = 0.2$.

Tests of an 0.88-inch-diameter static-pressure tube with four orifices on the top of the tube and seven on the bottom were conducted at $M = 0.6$ to 1.10 (ref. 18). The calibrations of this tube at $M = 0.6$, 0.8, and 1.0 (fig. 13) show the static-pressure errors to remain within 1 percent of $q_c$ of the value at $\alpha = 0^\circ$ for angles of attack up to $11^\circ$ at M between 0.6 and 1.0.

The effect of angle of attack on a 0.91-inch-diameter tube with four orifices on the top of the tube and six on the bottom was determined at supersonic speeds through an angle-of-attack range of $\pm 7^\circ$. The results, as presented in reference 7, showed that for this range of angle of attack, the static-pressure error remained within about 0.4 percent of $q_c$ of the $\alpha = 0^\circ$ value at $M = 1.62$ and 1.93.

## Conical Static-Pressure Tubes

Orifices on the surface of a cone have been proposed for the measurement of static pressure at supersonic speeds.

Experimental data for an orifice at two locations near the nose of a $3^\circ$ cone are presented in figure 14. These data were obtained from tests in the Langley 8-foot transonic tunnel at values of $\alpha$ between $1^\circ$ and $-1^\circ$ and $M = 0.20$ to 1.13. The calibrations show the static-pressure errors for the two orifice locations to remain within about 1 percent of $q_c$ over the range of Mach number tested.

Tests of orifices on a conical-nose body at $M = 1.59$ are reported in reference 19. In these tests four orifices were located 0.29 maximum body diameters from the front of a parabolic body of revolution with an apex angle of $15^\circ$. For the test Mach number (1.59) the results indicate that the static-pressure error is about 6 percent of $q$ at an angle of attack of $0^\circ$.

## Orifice Size and Configuration

The static-pressure errors due to the axial and circumferential location of the orifices, as discussed in the previous sections, apply to tubes with orifices which are accurately drilled and free from burs, protuberances, or depressions. Variations in the diameter and edge shape of the orifices can result in additional errors in the static-pressure measurements.

The influence of orifice diameter on the measured static pressure has been investigated with orifices on the inside wall of a cylindrical test section (ref. 20). The tests were conducted for orifice diameters of 0.006 to 0.125 inch over a Mach number range of about 0.4 to 0.8. The results of the tests at these two Mach numbers (fig. 15(a)) show the static-pressure error to increase with both orifice diameter and Mach number.

The effect of orifice diameter has also been determined for two orifice diameters on a 0.5-inch-diameter static-pressure tube at $M = 1.45$ (ref. 21). The results of these tests showed that an increase of 0.025 to 0.052 inch in the orifice diameter caused the static-pressure error to increase by 0.6 percent of $q_c$ at $\alpha = 0^\circ$.

In other tests of reference 20, the effect of varying the cross-sectional shape of the orifice edge was investigated with 0.032-inch-diameter orifices on the inside wall of a cylindrical test section. Sample results of these tests are presented in figure 15(b), which gives the difference between the static-pressure error of each orifice configuration and that of a sharp-edge orifice of the same diameter.

In reference 21, the effect of elongating the orifices in a 0.5-inch-diameter static-pressure tube was also investigated. The three configurations tested are shown in figure 15(c), and the differences in the static-pressure errors of the configurations, as referenced to a tube with 0.025-inch-diameter orifices encircling it, are given for the tubes at $\alpha = 0^{\circ}$ and $M = 2.55$ and 3.67.

## STATIC-PRESSURE ERRORS OF INSTALLATIONS

Static-pressure sources (tubes and vents) have been located at numerous positions on or near the aircraft. Static-pressure tubes have been located ahead of the fuselage nose, ahead of the wing, and ahead of the vertical tail fin. Static-pressure vents have generally been located on the fuselage between the nose and the wing or between the wing and the tail surfaces. The choice of type and location of the static-pressure source will depend on numerous considerations, such as the configuration and speed range of the aircraft, the accuracy required, pressure lag, icing, and the possibility of damage due to ground handling.

For any practical location of the static-pressure source, the installation will have a position error which will vary to some degree with Mach number and angle of attack. The position error will, therefore, vary with impact pressure, static pressure, aircraft weight, and normal acceleration. The error may also vary with changes in the configuration, and thus the flow field, of the aircraft - for example, changes in flap setting and landing-gear extension. As the flow field about an aircraft is markedly different for the subsonic, transonic, and supersonic speed ranges, the position errors for locations near the airplane may be expected to be quite different in each of the three speed ranges.

In the discussion to follow, the static-pressure errors of the various installations are presented as a function of Mach number or lift coefficient. Wherever possible, the effects of Mach number and lift coefficient have been separated. In those cases where the static-pressure errors of level-flight calibrations are plotted as a function of Mach number, the lift coefficient varies throughout the Mach number range. At the high subsonic and transonic Mach numbers at which these calibrations were performed, however, the variation of lift coefficient was small.

The static-pressure errors represent the overall static-pressure errors of the installation, that is, the sum of the position errors and the static-pressure errors of the pressure source. Diagrams of the static-pressure tubes used for the airplane installations are presented in figure 16, and the type of tube used with each installation is noted in the calibration figures.

## Static-Pressure Errors Ahead of Fuselage Nose

At Mach numbers below that at which a shock passes the static-pressure orifices, the position error at a given distance ahead of the fuselage nose is determined by the shape of the nose and the maximum diameter of the body.

Effect of nose shape.- The effect of nose shape was investigated in wind-tunnel tests of bodies of revolution (fineness ratio, 8.3) with circular, elliptical, elongated ogival noses (ref. 22). The tests were conducted at a Mach number of about 0.2 and at $\alpha = 0^{\circ}$. The results of the tests (fig. 17) show that, for a given distance ahead of the body, the position errors were greatest for the circular nose and least for the elongated ogival nose. At a distance of 1 diameter, for example, the errors were about 9, 4, and 1 percent, respectively, for the circular, elliptical, and elongated ogival noses. At 2 diameters the effect of variations in nose shape had diminished considerably.

The static-pressure errors at three distances ahead of a fuselage were measured on an airplane with an elliptical nose section (ref. 23). The results of these tests at small angles of attack ($C_L = 0.2$) are shown in figure 18 together with the data for the elliptical nose model taken from figure 17.

Effect of Mach number.- The effect of Mach number on the static-pressure errors ahead of two bodies of revolution at transonic speeds was determined by wing-flow tests (ref. 24). The nose shapes (that portion ahead of the maximum-diameter station) of the two bodies (fig. 19(a)) were similar. The nose shape of body A was developed from a circular arc, whereas the shape of body B was based on that of an actual airplane. The calibration of three installations on body B (fig. 19(a)) shows that, when the critical Mach number of the body is reached, the error begins to increase because the effect of negative pressures on the rear of the body are then diminished by the shock which forms around the maximum body diameter. When the free-stream Mach number becomes supersonic, a shock wave forms ahead of the body and the static-pressure error continues to increase as the shock moves toward the body. When the shock wave passes the orifices on the tube, the error falls to a value near zero, because the pressure field of the body is then isolated from the orifices. At the Mach number at which the shock wave passes the orifices, and at all higher Mach numbers, the pressure registered by the orifices should be that of the isolated tube. However, if the shock, after passing the orifices, interacts with the boundary layer to form a complex shock pattern in the vicinity of the orifices, the static-pressure error following the drop from the peak error will be slightly higher than that of the isolated tube. In this case, the static-pressure error will not return to that of the isolated tube until some higher Mach number has been reached.

In reference 24 it was shown that, for slender bodies having similar nose shapes, the position errors below the critical Mach number of the body and the peak errors just prior to the shock passage can both be correlated by the use of parameters which include the length as well as the diameter of the body. The manner in which the data of reference 24 correlate is shown in figure 19(b), which includes a theoretical curve for a parabolic-arc body calculated on the basis of the linearized subsonic theory. For the bodies considered, the peak errors are about twice the subsonic errors.

The calibration at transonic speeds of a static-pressure tube ahead of the nose of the airplane of which body B of figure 19 was a model (ref. 25) is presented in figure 20. These data confirm the results of the model tests by showing (1) the rapid increase in the static-pressure error at Mach numbers near 1.0, and (2) the discontinuity which occurs in the calibration when the fuselage bow wave passes the static-pressure orifices. The static-pressure errors of this airplane at values of M between 0.8 and 1.0 and those of a number of other airplanes with somewhat similar nose shapes (ref. 26) are plotted in figure 21 as a function of x/D. For a fuselage with a more elongated nose the static-pressure errors will, as shown in figure 22, be considerably lower (ref. 26).

The calibrations of fuselage-nose installations up to low supersonic speeds indicate that after the body bow wave and any boundary-layer—shock interaction have passed downstream of the orifices, the static-pressure error becomes that of the isolated tube and should remain at this value for all higher Mach numbers. That the static-pressure error remains small at higher supersonic speeds has been shown by calibration tests of a nose-boom installation on a free-flight rocket model. In this calibration, the error dropped to zero when the free-stream Mach number became supersonic and remained zero up to $M = 4.5$.

Effect of angle of attack.- The variation of static-pressure error with angle of attack for a number of positions ahead of bodies of revolution was investigated during the tests reported in reference 22. The results of these tests (fig. 23) show the error to decrease with increasing angle of attack. The change in static-pressure error for a given change in angle of attack is greatest near the nose and decreases with distance from the nose. At a distance of 1 diameter ahead of the nose, the change in static-pressure error for a change in angle of attack of $30^{\circ}$ is about 8 percent of $q_c$ for the circular nose, and 2 percent of $q_c$ for the elongated ogival nose.

In reference 27, the position errors ahead of slender parabolic-arc bodies of revolution at angles of attack were calculated on the basis of the subsonic linearized theory. Comparison between the theoretical and measured values for a body of revolution with a fineness ratio of 6 at

a Mach number of 0.2 showed the theory to be valid for distances greater than 0.5 body diameter ahead of the body and, for angles of attack less than $20^{\circ}$.

The effect of angle of attack on the static-pressure errors of fuselage-nose installations on airplanes at low and high subsonic speeds (refs. 23 and 25) is presented in figure 24. For lift coefficients up to 0.5, the effect of angle of attack is negligible. At $C_L$ above 0.5 the static-pressure errors of the installations on airplane A decrease with increasing $C_L$. However, for other combinations of fuselage-nose shape, boom length, orientation of orifices on static-pressure tube, and Mach number, the static-pressure error may increase at high angles of attack. (See ref. 26.)

Effect of nose inlet.- The position errors at various distances ahead of a body of revolution with a nose inlet were determined by wing-flow tests (ref. 24). The tests were conducted at transonic speeds and at $\alpha = 0^{\circ}$. The inlet velocity ratio varied from about 0.68 at $M = 0.7$ to 0.57 at $M = 1.0$. The results of the tests (fig. 25(a)) show the same general variation of static-pressure error with Mach number as the installations on sharp-nose bodies (fig. 19(a)). The variation of the static-pressure error at subsonic speeds ($M = 0.7$) with distance ahead of the body (fig. 25(b)) is also similar to that of the sharp-nose bodies. In other tests to determine the effect of inlet velocity, it was found that the static-pressure error increased when the inlet velocity ratio decreased.

Calibrations of nose-boom installations ahead of an airplane having a nose inlet (ref. 28) are given in figure 26. For these tests the orifices were located at various distances along a boom extending from the upper lip of the inlet. The calibrations of these installations exhibit the same variation of static-pressure error with Mach number as an installation ahead of a pointed-nose fuselage (fig. 20). The variation of the static-pressure errors with orifice location for a number of other airplanes with nose inlets is shown in figure 27 for $M = 0.80$ to 1.00.

## Static-Pressure Errors Ahead of Wings

Prior to the passage of the shock over the static-pressure orifices, the position error at a given distance ahead of the wing of an airplane depends on the shape of the airfoil section, the maximum thickness of the airfoil, the sweepback angle of the wing, and the spanwise location of the static-pressure tube. In order to avoid the influence of the fuselage and the wake of any propellers, static-pressure tubes are usually installed on the outboard span of the wing. The lengths of tubing between the static tube and the instruments, however, may create undesirable problems in pressure lag.

Effect of location of orifices.- Calibrations of static-pressure installations at various distances ahead of the leading edge of the wing tip of an unswept-wing airplane were determined at low subsonic speeds in reference 23. The variation of static-pressure error of these installations (at small angles of attack) with distance ahead of the wing, expressed as a multiple of the maximum wing thickness, is given in figure 28. At $x/t = 10$ (or 1 chord length for a 10-percent-thick airfoil), the error is about 1 percent, and it decreases only slightly with increasing distance ahead of the wing. The static-pressure errors of wing-tip installations on nine other unswept-wing airplanes with similar airfoil sections are also plotted in figure 28. This variation of static-pressure error with distance ahead of a wing tip is similar to that ahead of a transverse stem shown in figures 4 and 5.

Effect of Mach number (unswept wings).- The variation of static-pressure error with Mach number for a static-pressure tube located ahead of the wing tip of an unswept-wing airplane at transonic speeds (ref. 25) is presented in figure 29. The calibration of this installation is similar to that of the fuselage-nose installations up to the Mach number at which the discontinuity due to shock passage occurs. At this point, however, the error falls to a negative value and then, with increasing Mach number, begins to increase to positive values. The explanation for this behavior may best be illustrated by diagrams of the shock waves ahead of the airplane (fig. 30). At a Mach number of about 1.03, the wing bow wave has passed the orifices, thus effectively isolating them from the pressure field of the wing. At this Mach number, the pressure at the orifices is influenced by the negative pressures around the rear portion of the fuselage nose, the effect of which extends outward along Mach lines from the surface of the fuselage. As the Mach number increases, the Mach lines slant backward, and the orifices come under the influence of the positive pressures around the forward portion of the fuselage nose and behind the fuselage bow wave. At some higher Mach number, the fuselage bow wave will traverse the orifices, which will then be isolated from the flow fields of both wing and fuselage. At this and all higher Mach numbers, the static-pressure error will, in the absence of any boundary-layer—shock interaction, be that of the tube itself. It should be noted that, when the wing or fuselage bow shock is in the vicinity of the static-pressure orifices, the static-pressure error may vary considerably with angle of sideslip. For this reason a wing-tip installation at $M > 1.0$ is much more sensitive to angle of sideslip than a fuselage-nose installation.

Effect of angle of attack (unswept wings).- The variation of static-pressure error with lift coefficient at low subsonic Mach numbers (0.1 to 0.36) for various distances ahead of the wing tip of an unswept-wing airplane (ref. 23) is given in figure 31. These data show that, for lift coefficients up to 0.7, the effect of angle of attack is small for distances of $x/t = 4.2$ or greater. At higher lift coefficients, however, the effect of angle of attack is appreciable even for values of $x/t$ as large as 16.8.

The effect of angle of attack on the static-pressure errors of a wing-tip installation with $x/t = 4.1$ (ref. 29) at higher subsonic speeds (up to $M = 0.80$) is presented in figure 32. For the range of $C_L$ covered by the tests, the curves show that, at Mach numbers between 0.30 and 0.60, the static-pressure error decreases with lift coefficient. At $M = 0.70$, the effect of angle of attack is negligible, and with increasing Mach number (up to $M = 0.80$), the static-pressure error increases with lift coefficient.

Effect of Mach number (swept wings).- Calibrations of static-pressure tubes ahead of the wing tips of two swept-wing airplanes (refs. 30 and 31) are presented in figure 33. In one case the static-pressure tube was located 16t ahead of a 35° swept wing; in the other the tube was located 8.4t ahead of a 40° swept wing. The calibrations of these installations differ from those of wing-tip installations on unswept wings in that the static-pressure errors do not drop abruptly after the peak error is reached, but decrease toward zero at a more gradual rate.

Effect of angle of attack (swept wings).- The variation of static-pressure error with normal-force coefficient for a wing-tip installation on a swept-wing airplane at transonic speeds (ref. 30) is presented in figure 34. These data show that at $M = 0.75$ to 0.90 the static-pressure errors increase with angle of attack as in the case of the unswept-wing installation at $M = 0.75$ to 0.80 (fig. 32).

## Static-Pressure Errors Ahead of Vertical Tail Fin

Calibrations at transonic speeds of static-pressure tubes ahead of the tip of the vertical tail fins of two free-flight models are given in figure 35. One of these was a free-fall model of a canard airplane with the static-pressure orifices located 13.5t ahead of the tail fin. The other was a rocket-propelled model of an airplane configuration with the orifices 16.7t ahead of the tail fin. Although the magnitudes of the errors of both the installations are open to question (because of uncertainties in the telemetered measurements), the curves may be accepted as an approximate indication of the type of static-pressure-error variation to be expected for a vertical-tail-fin installation in the transonic speed range.

## Static-Pressure Errors of Vents on Fuselage (Models)

For the purpose of locating a fuselage static-pressure vent, the fuselage may, in a very general way, be likened to a static-pressure tube. As with the static-pressure tube, the pressure at a fuselage vent at zero angle of attack is determined by the axial location of the orifice along

the body. The pressure at a given point on the body may, of course, be modified by the blocking effect or the wake of any protuberances extending from the body. At angles of attack other than 0°, the pressure at a fuselage vent is, as with the static-pressure tube, determined by the circumferential orientation of the orifice.

Static-pressure vents have generally been located on opposite sides of the fuselage in order to minimize angle-of-sideslip effects. Calibrations, at angles of sideslip, of a vent installation in which two vents were located at approximately 67° and -67° on the bottom of a circular fuselage are reported in reference 32. The results showed that at an angle of sideslip of 4°, the maximum angle reached in the tests, the static-pressure error varied by 0.2 percent of $q_c$ from the value at zero angle of sideslip. When the cross section of the fuselage is circular, the orifices may also be located at approximately 30° and -30° on the bottom of the body to minimize angle-of-attack effects.

Because of the complex nature of the pressure distribution along the fuselage of an airplane, it is difficult to predict, with any degree of certainty, those locations where the static-pressure error will be minimum. It is customary, therefore, to make pressure-distribution tests in a wind tunnel with a detailed replica of the airplane, and to choose from the results a number of locations that appear promising for static-pressure vents. These locations are then calibrated on the full-scale airplane and the best location is chosen for the operational installation. In reference 33, the calibrations of fuselage-vent installations on a number of airplanes are compared with comparable installations on wind-tunnel models of these airplanes. For the low speeds at which these tests were conducted (below 175 knots), the results showed that the errors of the airplane installations could be predicted from the model tests to within ±2 percent of $q_c$.

Effect of axial location of vents.- Pressure-distribution studies of a body of revolution (ref. 34) provide a generalized indication of the pressure variation which might be expected along the fuselage of an airplane or missile. Sample results of these tests, which were conducted with a body of revolution with a fineness ratio of 12 at transonic speeds and at $\alpha = 0°$, are presented in figure 36. These curves show that for any given Mach number there are at least two axial locations, one on the forward portion and the other on the rearward portion of the fuselage, where the static-pressure error equals zero. It is evident, however, that these axial locations vary appreciably with Mach number.

Pressure-distribution tests of prolate spheroids (with aspect ratios of 6 and 10) and of a typical transonic body are reported in reference 35. In these tests the pressures over the forward half of the bodies were measured at $M = 0.3$ to 0.95 and at $\alpha = 0°$ to 7.7°.

Effect of Mach number.- The variation with Mach number of the static-pressure error of orifices at three axial locations along a body of revolution (ref. 34) is given in figure 37. These curves show that the magnitude and variation of static-pressure error change considerably along the body. In contrast to most of the static-pressure-tube installations, the variation of static-pressure error with Mach number for these vent installations is comparatively irregular. These variations, it must be remembered, apply to a simple body without protuberances of any kind. For an actual flight vehicle with wings, tail surfaces, external stores, and so forth, the pressure variation with Mach number can be expected to be much more complex.

The calibration of a vent on the cylindrical portion of the fuselage of a rocket-propelled model of an aircraft configuration at transonic and supersonic speeds is presented in figure 38. The single orifice was located on the top of the fuselage at 0.28 of the fuselage length behind the nose.

Effect of circumferential location of vents.- The possibility of minimizing the effect of angle of attack by properly locating the orifices around the circumference of a fuselage was investigated in reference 36. This study was based on tests with a body of revolution of fineness ratio 12.2 at $M = 1.59$ and at angles of attack up to $36^\circ$ (ref. 37). In this investigation (ref. 37) complete circumferential pressure distributions were obtained with orifices located at 12 stations along the body. The circumferential pressure distribution for an orifice located at the maximum-diameter station is given in figure 39 as a typical example of the results obtained. From these curves it would appear that the optimum location for static-pressure vents at this station would be about $\pm 40^\circ$ from the bottom of the body. For this orientation of the orifices, the static-pressure error remains within about 1/2 percent of $q_c$ of the value at $\alpha = 0^\circ$ (-3 percent of $q$) for angles of attack up to $20^\circ$. For the other axial locations tested, the optimum circumferential location and the range of angle of attack over which the error remained small differed from those at the maximum-diameter station.

## Static-Pressure Errors of Vents on Fuselage (Airplane)

An example of the type of calibration which may be expected for a static-pressure-vent installation at transonic speeds (ref. 30) is given in figure 40(a). The static-pressure vents of this installation were on each side of the nose of a jet fighter with a nose inlet and $35^\circ$ swept wings. The calibration of this installation showed the static-pressure error to change abruptly at a Mach number of about 0.98. This abrupt change is believed to be caused by passage of shock waves, which form in the local supersonic flow field around the nose of the fuselage, over the vents. The fact that the variations occur over a range of Mach

number (0.97 to 0.99) is probably due to asymmetry of the shock waves on each side of the fuselage which results from variations in angle of sideslip.

The effect of angle of attack on a fuselage vent (ref. 30) is shown in figure 40(b). At a Mach number of 0.75, the error begins to vary with normal-force coefficient at values of $C_N$ above 0.3. At the higher Mach numbers (M = 0.95) the effect of normal-force coefficient becomes evident at values of $C_N$ below 0.1. In comparison with the data of fuselage-nose and wing-tip boom systems on the same airplane (ref. 30), the fuselage-vent installation was shown to be affected to a much greater extent by angle of attack.

## Vent Configuration

The pressure registered by a fuselage static-pressure vent depends not only on its location on the fuselage but also on any protuberances or skin-contour variations in the vicinity of the orifice. The error of a vent installed on a pressurized fuselage may also change if the skin on which the vent is mounted flexes with pressurization.

Model tests of the effect of protuberances in the vicinity of a vent, waviness of the skin, and proximity of rivets are reported in reference 38. The results of these tests showed that relatively small imperfections in the surface surrounding the orifice can produce sizable changes in the position error. Sample data showing the effect of protuberances and skin waviness on the pressure of a 0.23-inch-diameter orifice at a speed of 175 knots are presented in figure 41.

For some fuselage-vent installations, specially designed protuberances have been installed near the vents in an attempt to compensate for the position errors at the vent location. Tests of several types of protuberances and indentations intended as aerodynamic compensators for fuselage vents are reported in reference 39.

## Conversion Factors

The static-pressure errors in this report have in most cases been expressed as a fraction of the impact pressure $q_c$. The errors are sometimes expressed in other nondimensional forms such as $\Delta p/p$ or $\Delta M/M$. For the convenience of the reader, a chart for converting $\Delta p/q_c$ to $\Delta p/p$ is given in figure 42. Charts from reference 40 for converting $\Delta p/q_c$ and $\Delta p/p$ to $\Delta M/M$ are presented in figure 43.

## COMPARISON OF INSTALLATIONS

As stated earlier, the choice of type and location of the static-pressure tube or vent depends on a number of factors. If the magnitude of the static-pressure error is the prime consideration, the selection will depend largely on the configuration of the aircraft and the speed range through which it is expected to operate.

A comparison of the calibrations of the various installations presented in this report indicates that, for an airplane designed to fly at supersonic speeds, a static-pressure tube located ahead of the fuselage nose will, in general, be the most desirable installation. This selection is based on the fact that the calibration has only one discontinuity (when the fuselage bow wave passes the orifices) and that at higher supersonic speeds the error will, for the usual case, be that of the isolated tube. In addition, the sensitivity of this installation to angle of sideslip at supersonic speeds will be that of the isolated tube. At subsonic and transonic speeds, the errors at a given distance ahead of the nose (in terms of fuselage diameters) depends on the shape of the nose section. As these errors decrease with increasing fineness ratio of the nose section, the static-pressure error of an installation ahead of a fuselage with a long pointed nose will be comparatively small throughout the speed range. An illustration of this fact may be seen from the calibration in figure 22. For installations ahead of blunter fuselage-nose sections, the errors at subsonic and transonic speeds will be considerably higher.

If the operating range of the airplane is confined to speeds below sonic, a static-pressure tube ahead of the wing tip may, for some airplane configurations, prove more satisfactory than a fuselage-nose installation. At equal distances ahead of the wing and fuselage nose, for example, the static-pressure error (at subsonic speeds) of the wing-tip installation will ordinarily be smaller than that of the fuselage-nose installation. The relative magnitudes of the errors of the two installations will, of course, depend on the relative values of the wing thickness and fuselage diameter and on the shape of the fuselage-nose section.

At speeds above sonic, a wing-tip installation will generally be less desirable than a fuselage-nose installation because of the relatively high sensitivity of the wing-tip installation to angle of sideslip, particularly at the Mach numbers at which the wing or fuselage shock waves are near the static-pressure orifices. In addition, the calibrations of wing-tip installations at supersonic speeds are more difficult to apply because of the two discontinuities which occur when the wing and fuselage bow waves pass the orifices.

For operation in the subsonic speed range, a static-pressure-tube installation ahead of a vertical tail fin may, for some configurations, offer certain advantages. In comparison with a wing-tip installation, for example, the thinner sections of vertical tail fins permit the use of shorter booms to achieve an equivalent static-pressure error. Because of the complex nature of the shock waves which form on the wing and fuselage, however, it would appear advisable to limit the use of vertical-tail-fin installations to Mach numbers below approximately 0.8.

Subsonic calibrations of numerous fuselage-vent installations on airplanes (not included in this report) have demonstrated that acceptable static-pressure errors can be obtained through a Mach number range up to about 0.8. The model tests presented in figure 37, however, showed irregular variations of static-pressure error with Mach number at transonic speeds. Furthermore, if the vents are near the fuselage nose, the static-pressure errors, as shown on figure 40, are apt to fluctuate erratically because of variations in angle of sideslip. It may be concluded, therefore, that fuselage vents, properly located and installed, may provide satisfactory calibrations at subsonic speeds up to $M = 0.8$.

## FLIGHT CALIBRATION METHODS

The calibration of an airspeed installation is usually accomplished by determining the errors in the pitot and static systems independently. The pitot system can be calibrated quite simply by comparison with a free-swiveling total-pressure tube or a shielded tube (of the type described in ref. 2) installed on the test airplane. The total-pressure error of the system being calibrated can be determined with a high degree of accuracy, since the difference between the total pressures of the two tubes can be measured directly with a differential pressure indicator or recorder.

The calibration of the static-pressure system may be performed by any one of a number of methods of varying degrees of complexity and accuracy. The choice of the calibration method will, in general, depend on the instrumentation available, the accuracy required, and the ranges of speed and lift coefficient over which the airplane is to be calibrated. As the procedure and instrumentation of most of the methods is quite involved, only a general description of each of the methods will be given here. Detailed information may be obtained by reference to the original reports.

### Speed-Course Method

In the speed-course method, the true airspeed of the airplane is determined by measuring the time required for the airplane to fly at constant speed and constant altitude between two landmarks (ref. 41). The effects of winds must be accounted for either by direct measurement or by elimination (by flying a triangular course or by flying in opposite directions along a straight-line course). The static-pressure error is determined by comparing the measured indicated airspeed with the correct indicated air speed (as computed from the measured true speed). The method is limited to speeds above the stall region and to the maximum speed of the airplane in level flight. The accuracy of the method is largely dependent on the accuracy of the measurement of time, the constancy of the wind speed, and the degree to which constant airspeed is maintained throughout the test.

### Trailing-Static-Tube Method

The static pressure of the static-pressure installation is compared directly with free-stream static pressure as measured by a static-pressure tube suspended on a long cable below the airplane (ref. 42). The cable must, of course, be long enough to place the trailing tube at a distance below the airplane where the pressure is approximately ambient. In reference 42, it was shown that the cable length should be approximately $1\frac{1}{2}$ to 2 wing spans. The advantage of this calibration method is that the calibration can be conducted at altitude and at speeds down to the stall. The maximum speed at which the tests may be conducted is limited by the speed at which the trailing tube encounters instability. The unstable motions of the towed body which develop above this limiting airspeed have been attributed to cable oscillations which originate near the airplane and are amplified by aerodynamic forces as they travel down the cable (ref. 43). Simple trailing tubes which depend on the weight of the body to keep them below the airplane have a maximum usable speed of approximately $M = 0.4$. A more complex trailing tube with wings set at a negative angle of incidence to keep it below the airplane has been towed to a Mach number of 0.85 (ref. 29). The accuracy which can be achieved by this method is relatively high because the difference between the system and free-stream pressures can be measured directly with a differential pressure instrument.

### Aneroid Method

Basically, the aneroid method consists in measuring the static pressure developed by the static-pressure system of the airplane at a known height and measuring the free-stream static pressure at the same

height. The static-pressure error of the installation is then determined as the difference between these two pressures. The pressure developed by the static-pressure tube may be measured either with an absolute-pressure gage or with an altimeter. The measurement of the reference height and of the free-stream static pressure at this height may be accomplished by any one of a variety of methods to be described.

Reference landmark.- The simplest form of the aneroid method is that in which the reference height is established as the top of a tall tower or building of known height (ref. 44). The free-stream static pressure at the reference height may be determined directly with an absolute-pressure gage or altimeter located at the top of the landmark. This measurement may also be determined by measuring the atmospheric pressure and temperature at the ground and computing the pressure at the reference height on the basis of the standard lapse rate. The flight calibration procedure consists in measuring the static pressure of the airplane installation as the airplane flies past the landmark in level flight at constant speed. Any deviations in the height of the airplane above or below the reference height may be determined either by visual observation or by photographing the airplane from the landmark. The speed range of the calibration is limited to speeds above the stall and below the maximum level-flight speed of the airplane. Because of the ease and precision with which the reference height and the free-stream static pressure can be measured, the static-pressure error of the installation may be determined with a relatively high degree of accuracy. The principal disadvantages of this method are the fact that the calibration is limited to level-flight speeds and the hazards involved in flying the airplane near the ground.

Photographic.- The height of the airplane may be determined either by photographing the airplane as it passes over a camera directed vertically upward from the ground or by photographing reference landmarks on the ground with a camera pointed vertically downward from the airplane. In either case, the height of the airplane is calculated from the focal length of the camera and a comparison of the size of the image on the film with the true dimensions of the object. For accurate measurements, corrections must be applied for any deviations of the airplane from zero angle of bank. The free-stream static pressure at the reference height is computed by using the standard lapse rate and measurements of pressure and temperature at the ground. Because the accuracy of the determination of free-stream static pressure by means of these computations decreases as the altitude of the airplane is increased, it may be advisable in some cases to determine the stream pressure by flying the airplane at a speed for which the installation has been previously calibrated by another method, for example, the reference-landmark method.

The calibration procedure consists in flying the airplane at constant speed and altitude over the ground station. Although the speed range of

the calibration is the same as that of the reference-landmark method, this method is less hazardous because the tests can be conducted at higher altitudes. In one application of this method, satisfactory calibrations have been made at heights of 300 to 800 feet (ref. 45). An attempt to use the method at much higher altitudes (25,000 to 30,000 feet) did not prove very successful (ref. 46).

Geometric.- In the first of two forms of the geometric method (described in ref. 47), the height of the airplane is determined by flying the airplane at constant speed and altitude over a predetermined ground course such as a line down a runway, and in measuring the elevation angle of the airplane from a ground station that is a known distance from the ground course. For best results, the distance of the ground station from the ground course should be about the same as the height at which the airplane is expected to fly. The elevation angle of the airplane may be determined with either a visual indicator (sighting stand of ref. 47) or a phototheodolite. Lateral deviations of the flight path of the airplane from the ground course must be estimated and corrected.

A second, and more accurate, form of this method involves the determination of the elevation angle of the airplane from two ground stations located a known distance apart and preferably an equal distance on each side of the ground course (ref. 47). This method has an advantage in that the flight path of the airplane may deviate from the ground course without affecting the accuracy of the height measurement. In either of these methods the free-stream static pressure at the reference height is calculated by using the standard lapse rate and measurements of pressure and temperature at some reference point on the ground, or it is measured by flying the airplane at a speed for which the calibration has been determined by other means.

Reference airplane.- The reference height may be established by another airplane flying at a low and constant speed and at constant pressure altitude (refs. 44 and 48). The static-pressure system of the reference airplane must have been previously calibrated for the speed at which it is flown in order to determine the free-stream static pressure at the reference height. The test airplane is then flown at a series of constant speeds past the reference airplane. Corrections for any differences between the height of the two airplanes can be determined most accurately by photographing the test airplane as it flies past the reference airplane.

Radar phototheodolite.- In another form of the aneroid method, the height of the airplane is calculated from the slant range and elevation angle of the airplane as measured by a radar-phototheodolite assembly located at a ground station (ref. 40). The radar antenna is directed at the test airplane by a separate optical tracking unit operated through a servo system. The radar-phototheodolite assembly consists of a radar

unit which has been modified by the addition of (1) an elevation scale on the radar antenna and a camera to photograph this scale and (2) a camera with a long-focal-length lens mounted at the center of, and boresighted with, the radar antenna. The scale camera provides a measure of the elevation angle of the optical axis of the antenna camera, and the antenna camera provides a means of correcting for any deviations of the position of the airplane from the optical axis of the antenna camera. A third camera is installed in the radar unit to photograph the range scope. The three cameras, together with the pressure-recording instruments in the airplane, are all synchronized by means of radio time signals transmitted from the airplane.

As this method permits calibrations of the airplane in dives and maneuvers as well as in level flight, the tests are usually conducted over a range of altitude. The free-stream static pressure at the reference altitudes must, therefore, be determined by measuring the variation of pressure with height over the test altitude range. This variation of pressure with height may be determined by any of the following methods:

(1) The test airplane is tracked by the radar phototheodolite as the airplane climbs through the test altitude range at a low, constant speed for which the static-pressure error has been determined by other means. The airplane is then flown through the same atmosphere at the higher speeds at which the installation is to be calibrated. For best results it is advisable to repeat the survey after the calibration runs have been made.

(2) For cases in which the airplane cannot be flown through the test altitude range at flight conditions (Mach number and lift coefficient) for which the calibration is known, the free-stream static pressure at one height (as measured by the radar phototheodolite) is first determined for one flight condition for which the static-pressure error is known (ref. 49). The airplane is then tracked by radar at other speeds through the test altitude range. From measurements of temperature and pressure during this ascent, the pressure $p_2$ at any given height $h_2$ may be determined by means of the following equation:

$$\left(\frac{p_2}{p_1}\right)^n = 1 - n\int_{h_1}^{h_2}\left(\frac{p'}{p_1}\right)^n \frac{1 + \frac{\gamma - 1}{2}K(M')^2}{RT'}\,dh \qquad (1)$$

where $p_1$ is the free-stream pressure at the start of the test (at altitude $h_1$), $p'$ and $T'$ are the measured pressure and temperature at altitude $h$, and $M'$ is the Mach number determined from the measured total pressure and the static pressure $p'$. The value of $n$ depends

on the temperature recovery factor K of the thermometer and on the Mach number. For K = 1, a value of n of $\frac{\gamma - 1}{\gamma}$ (or 0.286) gives satisfactory results at subsonic and low supersonic speeds. Computations of n for other values of K and M are given in reference 49.

(3) A radiosonde transmitting pressure measurements is tracked by the radar phototheodolite through the test altitude range (ref. 50). The calibration tests of reference 50 indicated that the static-pressure measurements from the radiosonde were not sufficiently accurate to establish the static-pressure error of the installation to the required accuracy.

(4) The variation of pressure with height at the test altitudes is computed from measurements of temperature and pressure transmitted from a radiosonde (ref. 50). The height at any given pressure level may be computed from the equation

$$h = -\int_0^h \frac{RT}{p}\,dp \qquad (2)$$

where p and T are simultaneous radiosonde measurements. This equation indicates that an error in static pressure results in an error in altitude of opposite sign. Therefore, in a plot of pressure against altitude, the error in altitude tends to compensate for the error in static pressure. As a consequence, the variation of static pressure with altitude obtained by this method will be closer to the actual variation than that obtained when the static pressure is measured by the radiosonde and the height of the radiosonde is measured by a radar theodolite.

Radio altimeter.- The reference height is determined by means of a radio altimeter installed in the airplane (ref. 51). The variation of free-stream static pressure with height is first determined by flying the airplane through the test altitude range at a low constant speed for which the static-pressure error is known. The calibration tests are then performed through the same atmosphere, the height of the airplane being measured by the radio altimeter.

Like the radar-phototheodolite method, this method allows the calibrations to be conducted at high altitude. The instrumentation required for this method, however, is much simpler and has the advantage of being entirely contained within the airplane. The method has the disadvantage of requiring a level ground-reference plane, and thus it is restricted to flight over a large body of water. From the tests reported in reference 51, the accuracy of this method was found to be of the same order as that of the radar-phototheodolite method. Another evaluation of this method is reported in reference 52.

Accelerometer.- In the accelerometer method (ref. 49), the free-stream static pressure at a given height is determined by flying the airplane in level flight at a speed for which the static-pressure error has previously been determined by another method. The airplane is then flown in level flight or in vertical-plane maneuvers at the higher speeds for which a calibration is desired. From measurements of normal and longitudinal acceleration and the attitude angle of the airplane, a calculation is made of the vertical velocity which, when integrated, provides a measure of the change in height. The height increment is then combined with temperature measurements to determine the variation of free-stream static pressure with height during the calibration run. An evaluation of this method (ref. 49) as compared with the radar-phototheodolite method showed the accuracy of the two methods to be comparable.

## Radar-Temperature Method

In the radar-temperature method (ref. 50), the variation of ambient temperature with height is first determined by (1) tracking a radiosonde (transmitting temperature measurements) with a radar phototheodolite or (2) computing the height of the radiosonde from equation (2) using values of pressure and temperature transmitted from the radiosonde. The test airplane is then tracked by the theodolite as the airplane is flown through the atmosphere surveyed. During the calibration runs continuous measurements are made of the total temperature developed by a probe on the airplane. From a knowledge of the total temperature $T'$ and the ambient temperature $T$ at a given height, the true Mach number at this height may be determined from the equation

$$\frac{T'}{T} = 1 + 0.2KM^2 \qquad (3)$$

From a comparison of the true Mach number with the Mach number measured by the airplane installation at this height, the static-pressure error may be calculated. The accuracy which may be obtained with this method is discussed in reference 50.

## Temperature Method

This method is based on the assumption that the temperature and pressure at a given point in the atmosphere remains unchanged over a short period of time. The method, as described in reference 53, consists in measuring the temperature, static pressure, and total pressure from the airplane as it is flown through the test altitude range at a speed for which the calibration is known. This survey establishes the relation between the ambient temperature and the free-stream static pressure. The airplane is then flown through the altitude range surveyed, and the same measurements are repeated. The values of the indicated

temperature and total pressure at a given instant in the calibration run, together with the temperature recovery factor of the thermometer, define the relation between the ambient temperature and the indicated static pressure at that instant. From a comparison of this temperature with the temperature-pressure variation determined in the survey, the free-stream static pressure at that instant is determined. The static-pressure error is then found as the difference between the indicated and free-stream static pressures. Although the instrumentation required for this method is comparatively simple, the measurement of temperature must be very precise. The accuracy which may be obtained with this method was determined in the tests reported in reference 54.

### Formation-Flight Method

In the formation-flight method, the test airplane is flown in formation with another airplane that has a calibrated airspeed system. The static-pressure error may be determined by comparing either the altimeter or the airspeed indicator readings of the two aircraft. If airspeed readings are compared, the errors, if any, in the total-pressure systems of the two airplanes must be taken into account. This method is limited to the altitude and speed capabilities of the reference airplane. An evaluation of the accuracy which may be achieved with this method at speeds between 200 and 400 knots is reported in reference 55.

## CONCLUDING REMARKS

From a comparison of the calibrations of four types of static-pressure-measuring installations (fuselage nose, wing-tip, vertical tail fin, and fuselage vent) the following conclusions may be drawn:

1. For an airplane designed to operate at supersonic speeds, a static-pressure tube located ahead of the fuselage nose will, in general, be the most desirable installation.

2. If the operating range is confined to speeds below sonic, a static-pressure tube located ahead of the wing tip may, for some airplane configurations, prove more satisfactory than a fuselage-nose installation.

3. For operation at Mach numbers below 0.8, a static-pressure tube ahead of the vertical tail fin or fuselage vents, properly located and installed, should prove satisfactory.

Langley Aeronautical Laboratory,
National Advisory Committee for Aeronautics,
Langley Field, Va., December 17, 1956.

## REFERENCES

1. Huston, Wilber B.: Accuracy of Airspeed Measurements and Flight Calibration Procedures. NACA Rep. 919, 1948. (Supersedes NACA TN 1605.)

2. Gracey, William: Wind-Tunnel Investigation of a Number of Total-Pressure Tubes at High Angles of Attack - Subsonic, Transonic, and Supersonic Speeds. NACA TN 3641, 1956.

3. Taback, Israel: The Response of Pressure Measuring Systems to Oscillating Pressures. NACA TN 1819, 1949.

4. Smith, Keith: Pressure Lag in Pipes With Special Reference to Aircraft Speed and Height Measurements. Rep. No. Aero 2507, British R.A.E., Nov. 1954.

5. Kumbruch, H.: Pitot-Static Tubes for Determining the Velocity of Air. NACA TM 303, 1925.

6. Lock, C. N. H., Knowler, A. E., and Pearcey, H. H.: The Effect of Compressibility on Static Heads. R. & M. No. 2386, British A.R.C., Jan. 1943.

7. Hasel, Lowell E., and Coletti, Donald E.: Investigation of Two Pitot-Static Tubes at Supersonic Speeds. NACA RM L8I02, 1948.

8. Walter, L. W., and Redman, E. J.: Needle Static-Pressure Probes Insensitive to Flow Inclination in Supersonic Air Streams. NAVORD Rep. 3694 (Aeroballistic Res. Rep. 231), U.S. Naval Ord. Lab. (White Oak, Md.), Mar. 15, 1954.

9. Holder, D. W., North, R. J., and Chinneck, A.: Experiments With Static Tubes in a Supersonic Airstream - Parts I and II. R. & M. No. 2782, British A.R.C., July 1950.

10. Hensley, Reece V.: Calibrations of Pitot-Static Tubes at High Speeds. NACA WR L-396, 1942. (Formerly NACA ACR, July 1942.)

11. Stivers, Louis S., Jr., and Adams, Charles N., Jr.: High-Speed Wind-Tunnel Investigation of the Effects of Compressibility on a Pitot-Static Tube. NACA RM A7F12, 1947.

12. Merriam, Kenneth G., and Spaulding, Ellis R.: Comparative Tests of Pitot-Static Tubes. NACA TN 546, 1935.

13. Bursnall, William J., and Loftin, Laurence K., Jr.: Experimental Investigation of the Pressure Distribution About a Yawed Circular Cylinder in the Critical Reynolds Number Range. NACA TN 2463, 1951.

14. Gowen, Forrest E., and Perkins, Edward W.: Drag of Circular Cylinders for a Wide Range of Reynolds Numbers and Mach Numbers. NACA TN 2960, 1953.

15. Smith, W. E.: Wind Tunnel Calibration of Two Static-Pressure Sensing Devices. Rep. No. AF-682-A-6 (WADC Contract No. AF 33(038)-10709), Cornell Aero. Lab. Inc., Dec. 1952.

16. Ziegler, Norman G.: Wind-Tunnel Calibration of the Given High-Speed Pitot-Static Probe at Mach Numbers of 1.57 and 1.88. Aero. Data Rep. 33, David Taylor Model Basin, U.S.N., Sept. 1955.

17. Gracey, William, and Scheithauer, Elwood F.: Flight Investigation at Large Angles of Attack of the Static-Pressure Errors of a Service Pitot-Static Tube Having a Modified Orifice Configuration. NACA TN 3159, 1954.

18. Pearson, Albin O., and Brown, Harold A.: Calibration of a Combined Pitot-Static Tube and Vane-Type Flow Angularity Indicator at Transonic Speeds and at Large Angles of Attack or Yaw. NACA RM L52F24, 1952.

19. Cooper, Morton, and Webster, Robert A.: The Use of an Uncalibrated Cone for Determination of Flow Angles and Mach Numbers at Supersonic Speeds. NACA TN 2190, 1951.

20. Rayle, Roy E., Jr.: An Investigation of the Influence of Orifice Geometry on Static Pressure Measurements. M. S. Thesis, M.I.T., 1949.

21. Buquoi, T. W., Lundquist, L. E., and Stark, J. M.: Presentation of Pressure Data From a Supersonic Wind Tunnel Configuration Study of a Full Scale Nike B Static Pressure Probe. Rep. No. SM-19228, Douglas Aircraft Co., Inc., Apr. 19, 1956.

22. Letko, William: Investigation of the Fuselage Interference on a Pitot-Static Tube Extending Forward From the Nose of the Fuselage. NACA TN 1496, 1947.

23. Gracey, William, and Scheithauer, Elwood F.: Flight Investigation of the Variation of Static-Pressure Error of a Static-Pressure Tube With Distance Ahead of a Wing and a Fuselage. NACA TN 2311, 1951.

24. O'Bryan, Thomas C., Danforth, Edward C. B., and Johnston, J. Ford.: Error in Airspeed Measurement Due to the Static-Pressure Field Ahead of an Airplane at Transonic Speeds. NACA Rep. 1239, 1955. (Supersedes NACA RM's L9C25 by Danforth and Johnston, L50L28 by Danforth and O'Bryan, and L52A17 by O'Bryan.)

25. Goodman, Harold R., and Yancey, Roxanah B.: The Static-Pressure Error of Wing and Fuselage Airspeed Installations of the X-1 Airplanes in Transonic Flight. NACA RM L9G22, 1949.

26. Larson, Terry J., Stillwell, Wendell H., and Armistead, Katharine H.: Static-Pressure Error Calibrations for Nose-Boom Airspeed Installations of 17 Airplanes. NACA RM H57A02, 1957.

27. Letko, William, and Danforth, Edward C. B., III: Theoretical Investigation at Subsonic Speeds of the Flow Ahead of a Slender Inclined Parabolic-Arc Body of Revolution and Correlation With Experimental Data Obtained at Low Speeds. NACA TN 3205, 1954.

28. Roe, M.: Position Error Calibration of Three Airspeed Systems on the F-86A Airplane Through the Transonic Speed Range and in Maneuvering Flight. Rep. No. NA-51-864, North American Aviation Inc., Oct. 5, 1951.

29. Smith, K. W.: The Measurement of Position Error at High Speeds and Altitude by Means of a Trailing Static Head. C.P. No. 160, British A.R.C., 1954.

30. Thompson, Jim Rogers, Bray, Richard S., and Cooper, George E.: Flight Calibration of Four Airspeed Systems on a Swept-Wing Airplane at Mach Numbers up to 1.04 by the NACA Radar-Phototheodolite Method. NACA TN 3526, 1955.

31. Andrews, D. R., and Nethaway, J. E.: Flight Measurements of the Pressure Errors of a Nose and a Wing Boom Airspeed System on a Swept-Wing Aircraft (Hunter F Mk. I) at Mach Numbers up to 1.2. Tech. Note No. Aero 2354, British R.A.E., Jan. 1955.

32. Chilton, Robert G., and Brown, B. Porter: Flight Investigation of the Effect of Sideslip on the Pressure at the Static Orifices of the Boeing B-29 Airplane. NACA RM L50J30, 1951.

33. Somerville, T. V., Kirk, F. N., and Jefferies, R. L.: Comparison of Model and Full Scale Tests on a Fuselage Vent for Measurements of Static Pressure. Rep. No. Aero 1806, British R.A.E., Mar. 1943.

34. Thompson, Jim Rogers: Measurements of the Drag and Pressure Distribution on a Body of Revolution Throughout Transition From Subsonic to Supersonic Speeds. NACA RM L9J27, 1950.

35. Matthews, Clarence W.: A Comparison of the Experimental Subsonic Pressure Distributions About Several Bodies of Revolution With Pressure Distributions Computed by Means of the Linearized Theory. NACA Rep. 1155, 1953. (Supersedes NACA TN 2519.)

36. Cooper, Morton, and Hamilton, Clyde V.: Orientation of Orifices on Bodies of Revolution for Determination of Stream Static Pressure at Supersonic Speeds. NACA TN 2592, 1952.

37. Cooper, Morton, Gapcynski, John P., and Hasel, Lowell E.: A Pressure Distribution Investigation of a Fineness-Ratio-12.2 Parabolic Body of Revolution (NACA RM-10) at $M = 1.59$ and Angles of Attack up to $36^{\circ}$. NACA RM L52G14a, 1952.

38. Somerville, T. V., and Jefferies, R. L.: Note on Model Tests of Static Vents. Effect of Degrees of Flushness, Waviness of Skin and Proximity of Rivets. B. A. Dept. Note - Wind Tunnels No. 531, British R.A.E., Sept. 1941.

39. Howard, J. R.: Wind Tunnel Tests of Alternate Static Source Protuberances for the F-86A Airplane. Rep. No. NA-49-449, North American Aviation, Inc., June 16, 1949.

40. Zalovcik, John A.: A Radar Method of Calibrating Airspeed Installations on Airplanes in Maneuvers at High Altitudes and at Transonic and Supersonic Speeds. NACA Rep. 985, 1950. (Supersedes NACA TN 1979.)

41. Thompson, F. L.: Procedure for Determining Speed and Climbing Performance of Airships. NACA TN 564, 1936.

42. Thompson, F. L.: The Measurement of Air Speed of Airplanes. NACA TN 616, 1937.

43. Phillips, William H.: Theoretical Analysis of Oscillations of a Towed Cable. NACA TN 1796, 1949.

44. Thompson, F. L., and Zalovcik, John A.: Airspeed Measurements in Flight at High Speeds. NACA A.R.R., Oct. 1942.

45. Hesse, W. J.: Position Error Determination by Stadiametric Ranging With a 35mm Movie Camera. Tech. Rep. No. 2-55, Test Pilot Training Div., U. S. Naval Air Test Center (Patuxent River, Md.), June 24, 1955.

46. Lang, D. W., and Charnley, W. J.: Measurement of Aircraft Height and Speed in High Speed Dives by a Photographic Method and by Radar Tracking. R. & M. No. 2351, British A.R.C., Jan. 1946.

47. Schoenfeld, L. I., and Harding, G. A.: Report on the Dual Sighting Stand and Other Methods of Calibrating Altimeter and Airspeed Installations. Rep. No. NAES-INSTR-16-44 (Project No. TED NAM 3335), NAES, Philadelphia Navy Yard, Aug. 15, 1944.

48. Fuhrman, R. A., Wheatley, J. P., Lytle, W. J., and Doyle, G. B.: Preliminary Report on Airspeed-Altimeter System Calibration at High Mach Numbers. Phase A - The Altimeter Depression Method Using a Base Airplane at Altitude. Test Pilot Training Div., U. S. Naval Air Test Center (Patuxent River, Md.), Mar. 3, 1952.

49. Zalovcik, John A., Lina, Lindsay J., and Trant, James P., Jr.: A Method of Calibrating Airspeed Installations on Airplanes at Transonic and Supersonic Speeds by the Use of Accelerometer and Attitude-Angle Measurements. NACA Rep. 1145, 1953. (Supersedes NACA TN 2099 by Zalovcik and NACA TN 2570 by Lina and Trant.)

50. Brunn, Cyril D., and Stillwell, Wendell H.: Mach Number Measurements and Calibrations During Flight at High Speeds and at High Altitudes Including Data for the D-558-II Research Airplane. NACA RM H55J18, 1956.

51. Thompson, Jim Rogers, and Kurbjun, Max C.: Evaluation of the Accuracy of an Aircraft Radio Altimeter for Use in a Method of Airspeed Calibration. NACA TN 3186, 1954.

52. Moroney, J. E.: A Method of Utilizing a Radio Altimeter to Determine Airspeed Calibrations of High Performance Airplanes at High Altitude by Use of the Altimeter Depression Method. Tech. Rep. No. 1-55, Test Pilot Training Div., U. S. Naval Air Test Center (Patuxent River, Md.), May 27, 1955.

53. Zalovcik, John A.: A Method of Calibrating Airspeed Installations on Airplanes at Transonic and Supersonic Speeds by Use of Temperature Measurements. NACA TN 2046, 1950.

54. Lina, Lindsay J., and Ricker, Harry H., Jr.: Measurements of Temperature Variations in the Atmosphere Near the Tropopause With Reference to Airspeed Calibration by the Temperature Method. NACA TN 2807, 1952.

55. Levon, K. C.: Pressure Error Measurement Using the Formation Method. C.P. No. 126, British A.R.C., 1953.

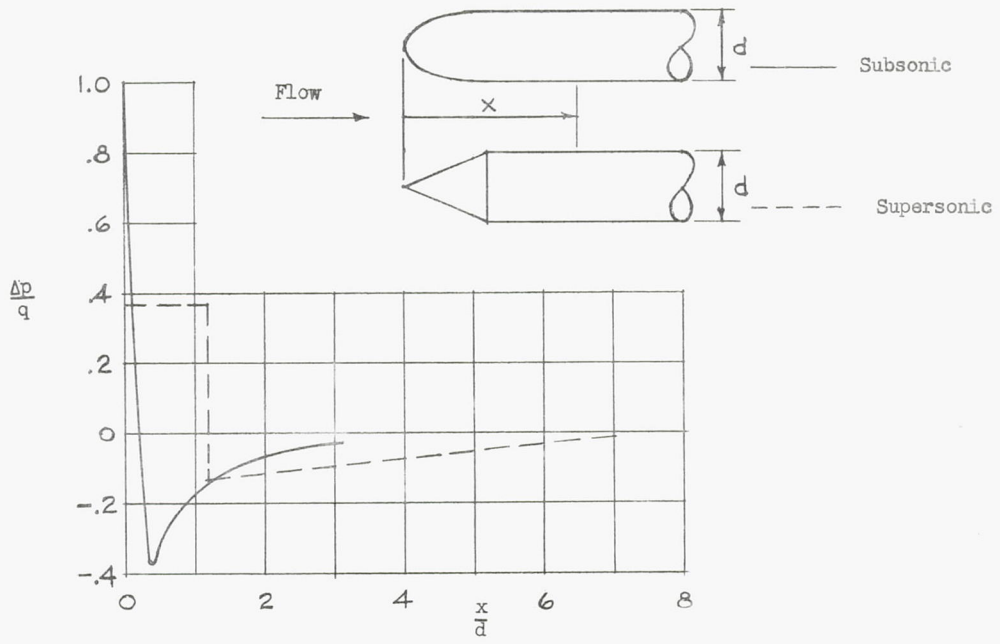


Figure 1.- Theoretical pressure distribution along cylindrical bodies (subsonic data from ref. 5).

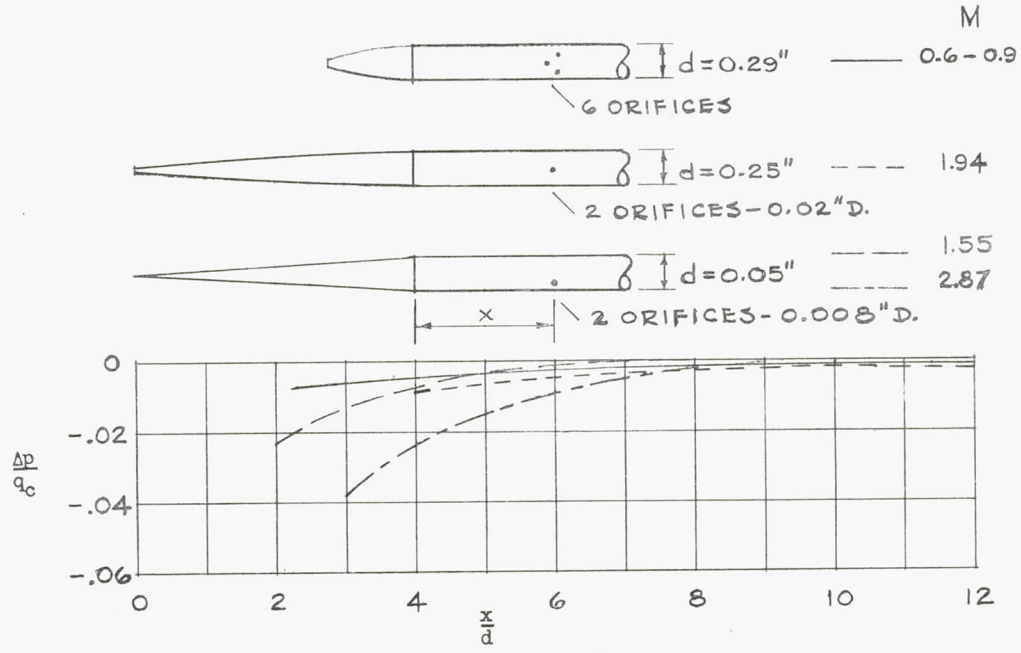


Figure 2.- Experimental pressure distribution along static-pressure tubes (refs. 6, 7, and 8).

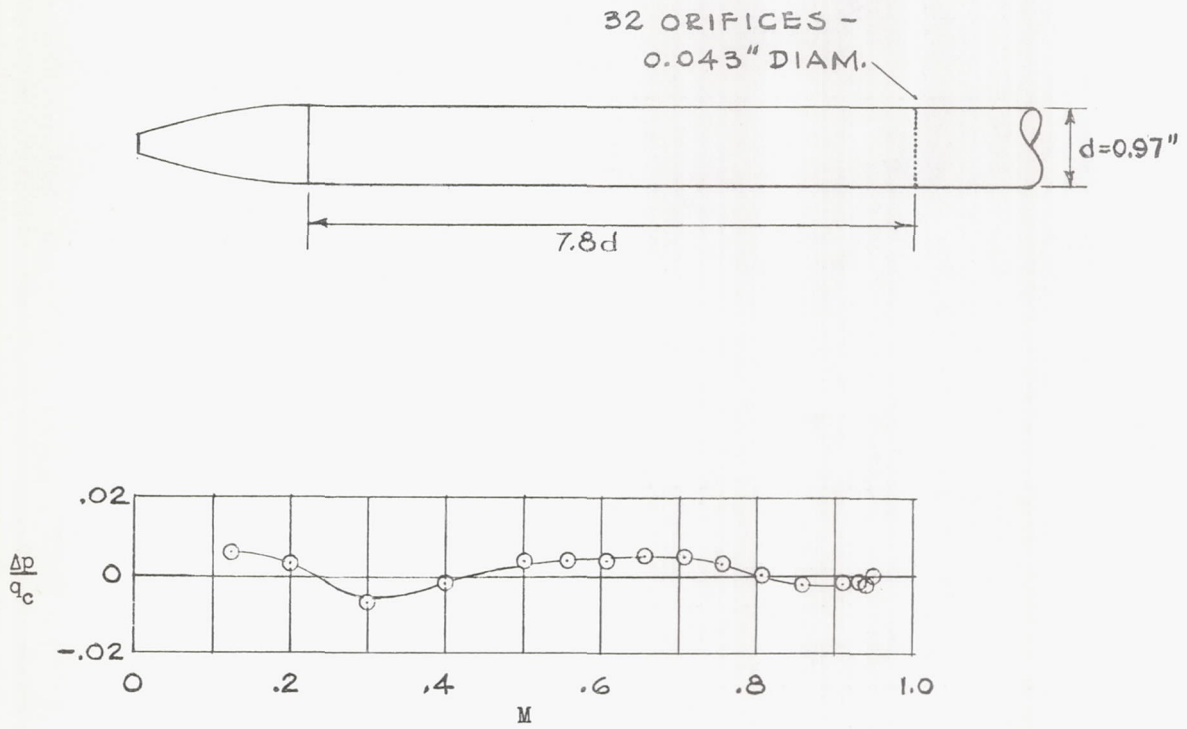


Figure 3.- Calibration of a static-pressure tube at $\alpha = 0^{\circ}$.

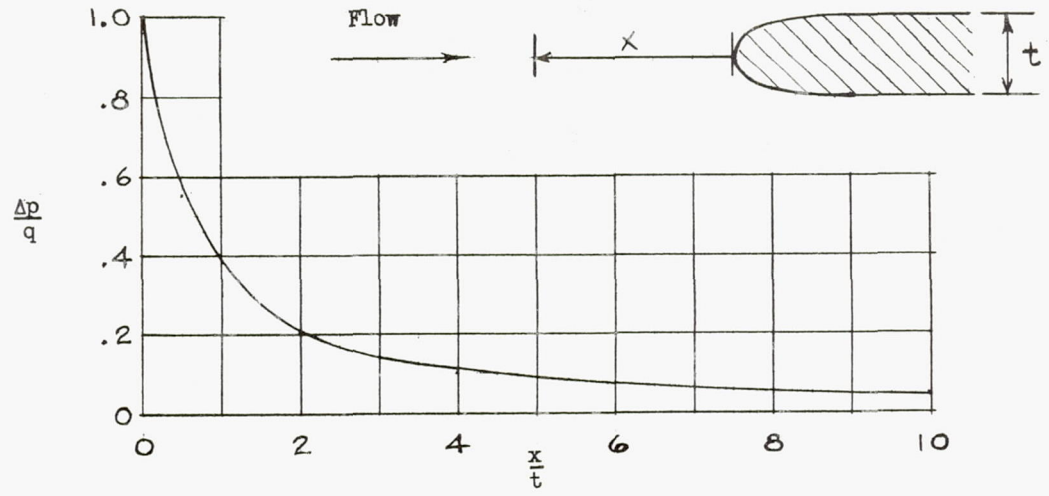


Figure 4.- Theoretical pressure distribution ahead of a body of infinite length transverse to the flow (incompressible-flow theory, ref. 5).

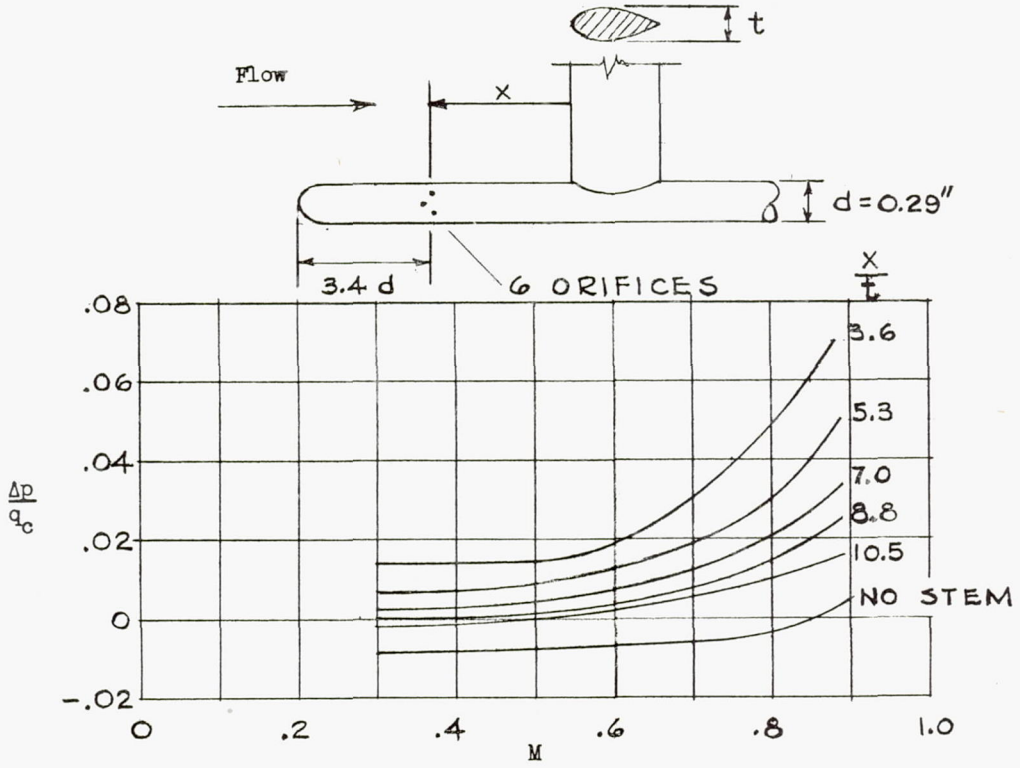


Figure 5.- Effect of transverse stem on the pressure developed by a static-pressure tube at $\alpha = 0^{\circ}$ (ref. 6).

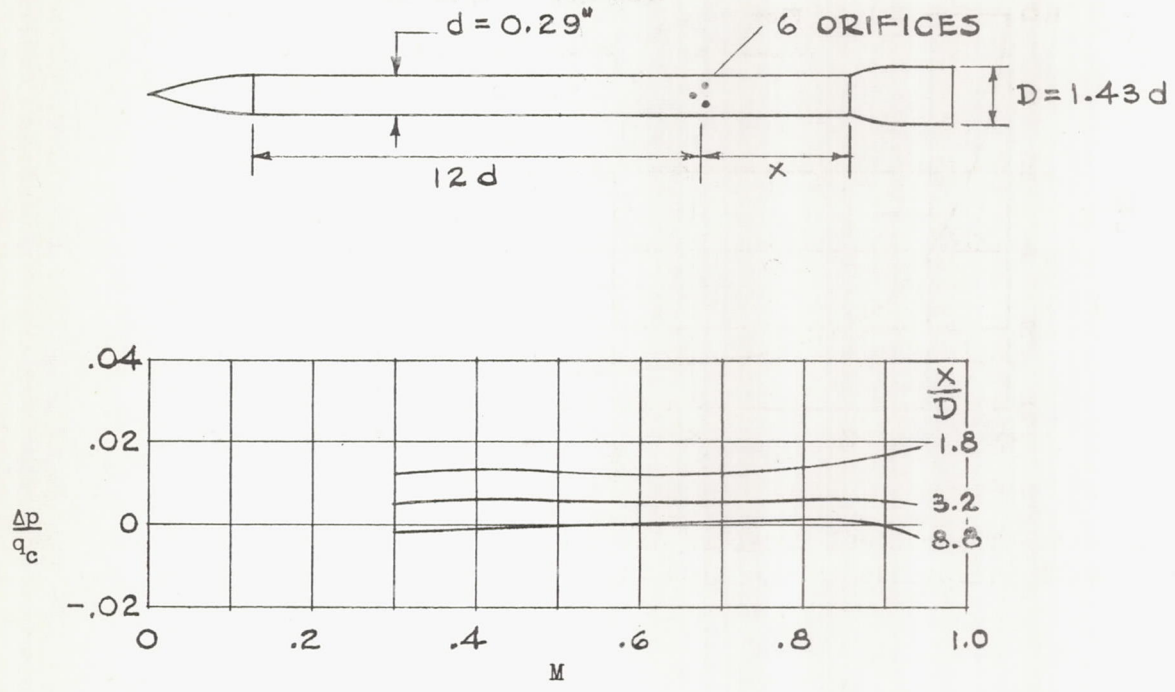


Figure 6.- Effect of collar on the pressure developed by a static-pressure tube at $\alpha = 0^{\circ}$ (ref. 6).

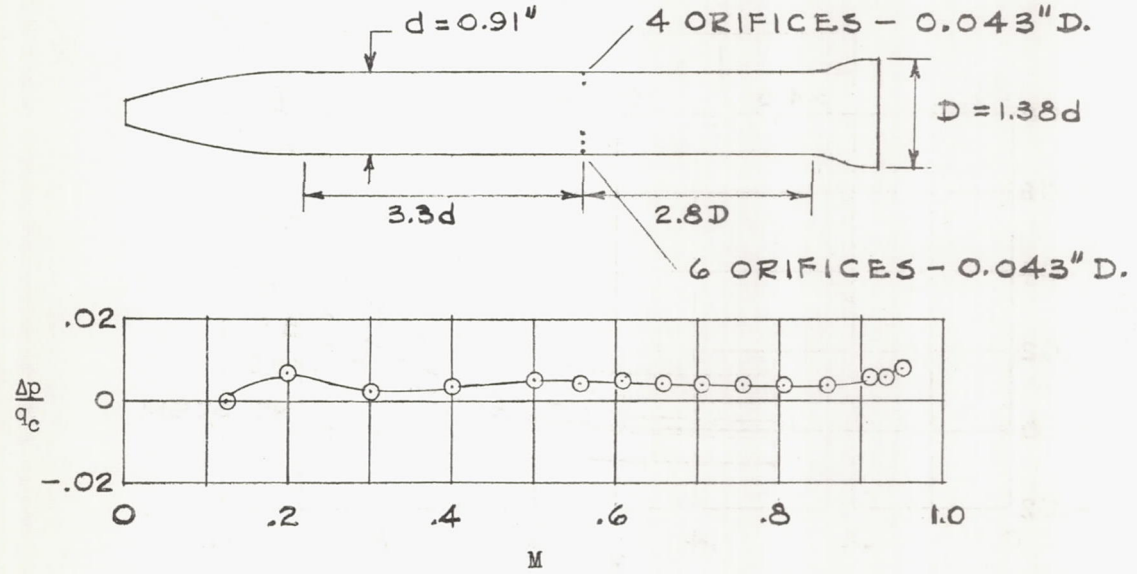


Figure 7.- Calibration of a static-pressure tube with collar at $\alpha = 0^{\circ}$.

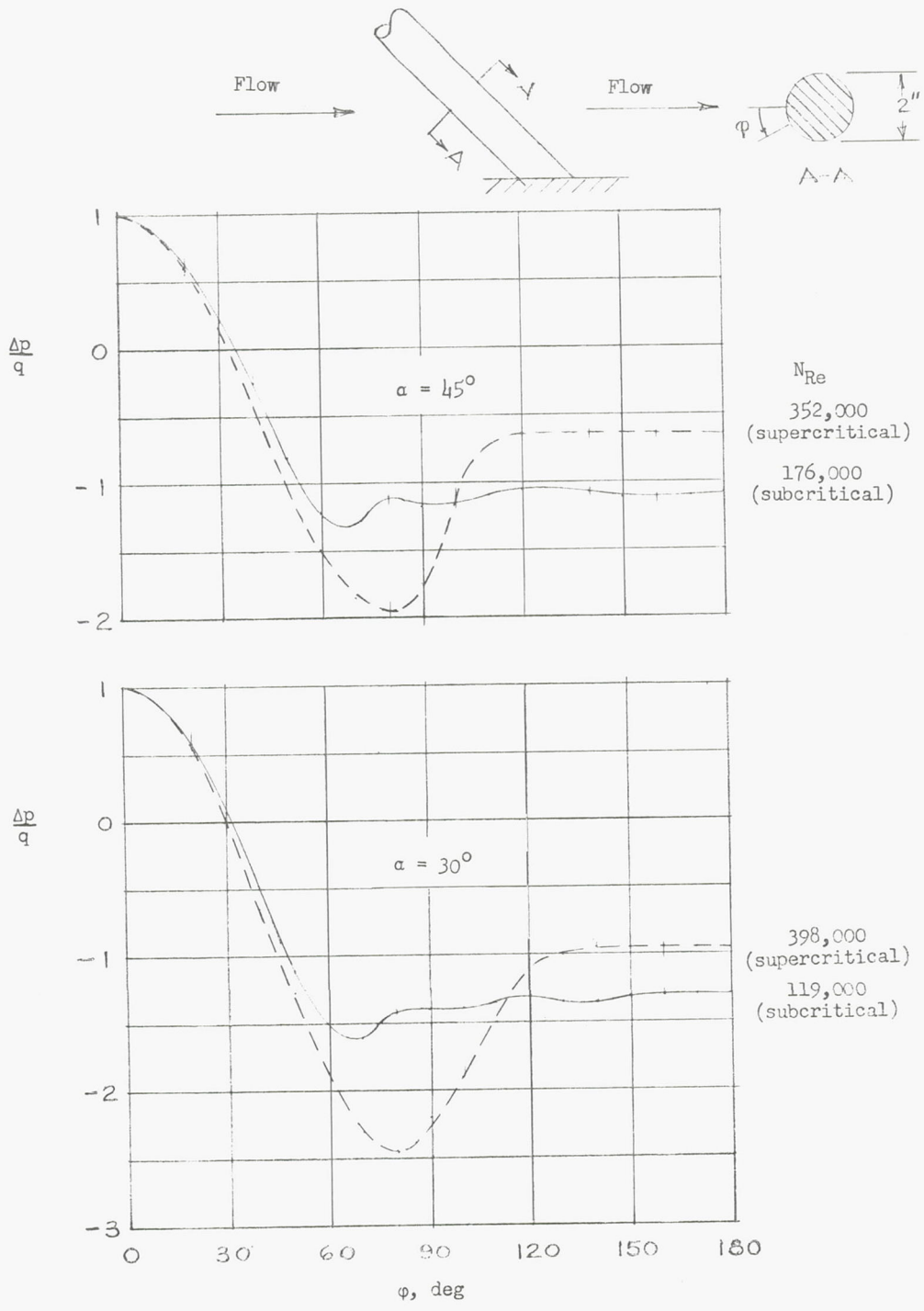


Figure 8.- Pressure distribution around a cylinder at angles of attack of 30° and 45° (ref. 13).

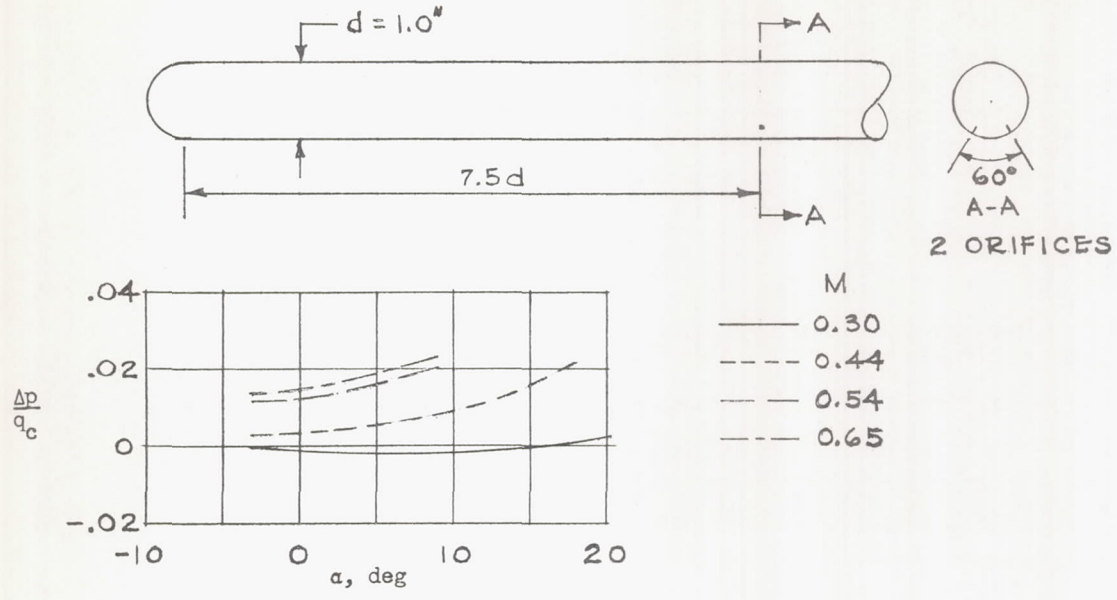


Figure 9.- Calibration at angles of attack of a static-pressure tube with orifices at circumferential stations of 30° and -30° (ref. 15).

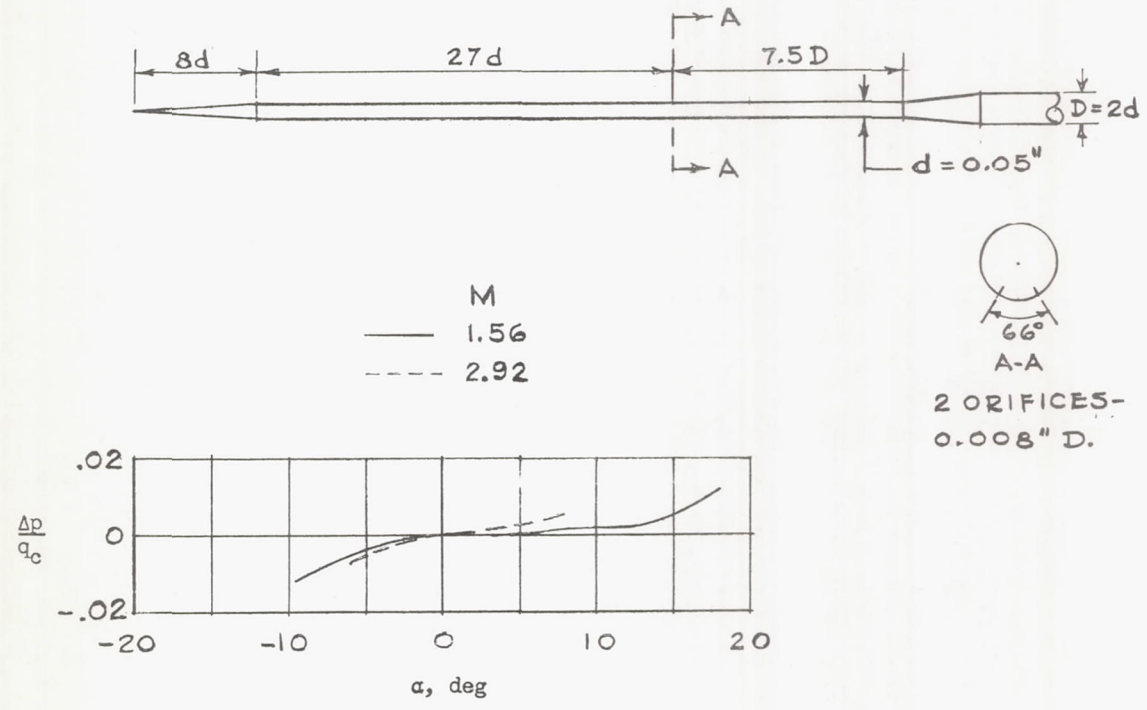


Figure 10.- Calibration at angles of attack of a static-pressure tube with orifices at circumferential stations of 33° and -33° (ref. 8).

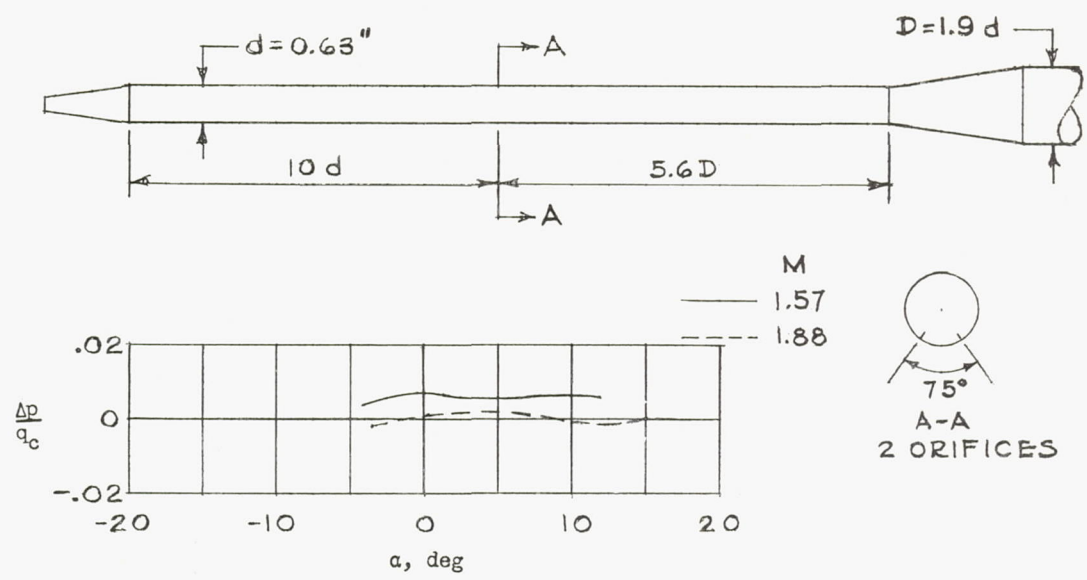


Figure 11.- Calibration at angles of attack of a static-pressure tube with orifices at circumferential stations of 37.5° and -37.5° (ref. 16).

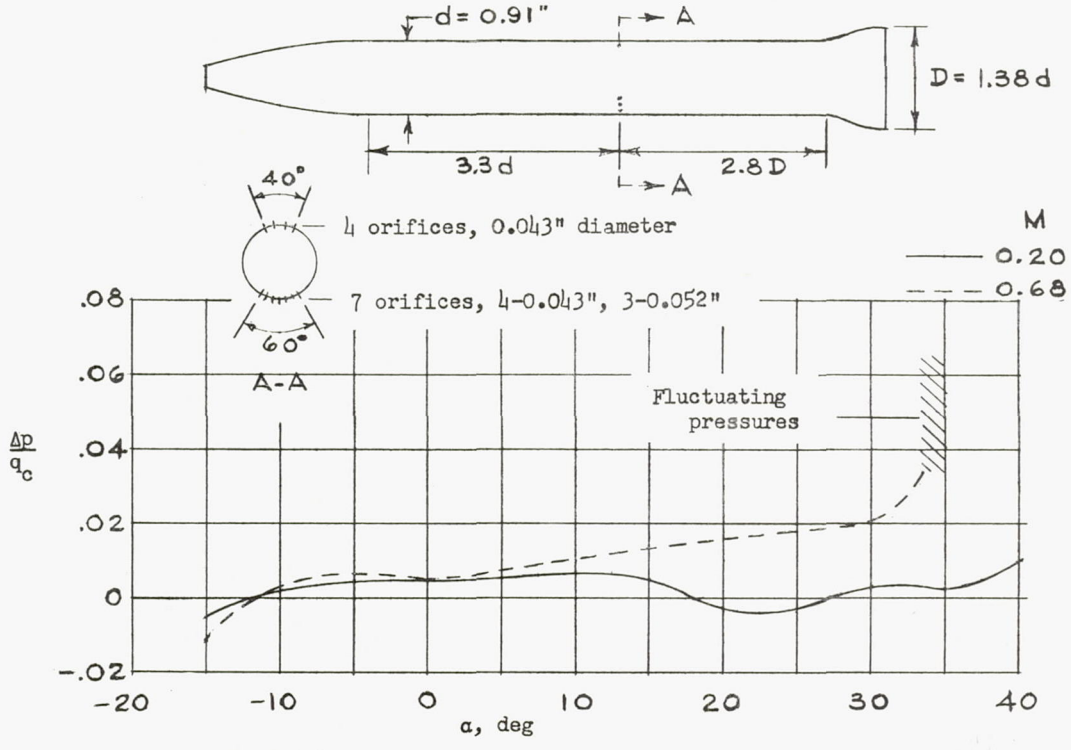


Figure 12.- Calibration at angles of attack of a static-pressure tube with an unsymmetrical orifice arrangement (ref. 17).

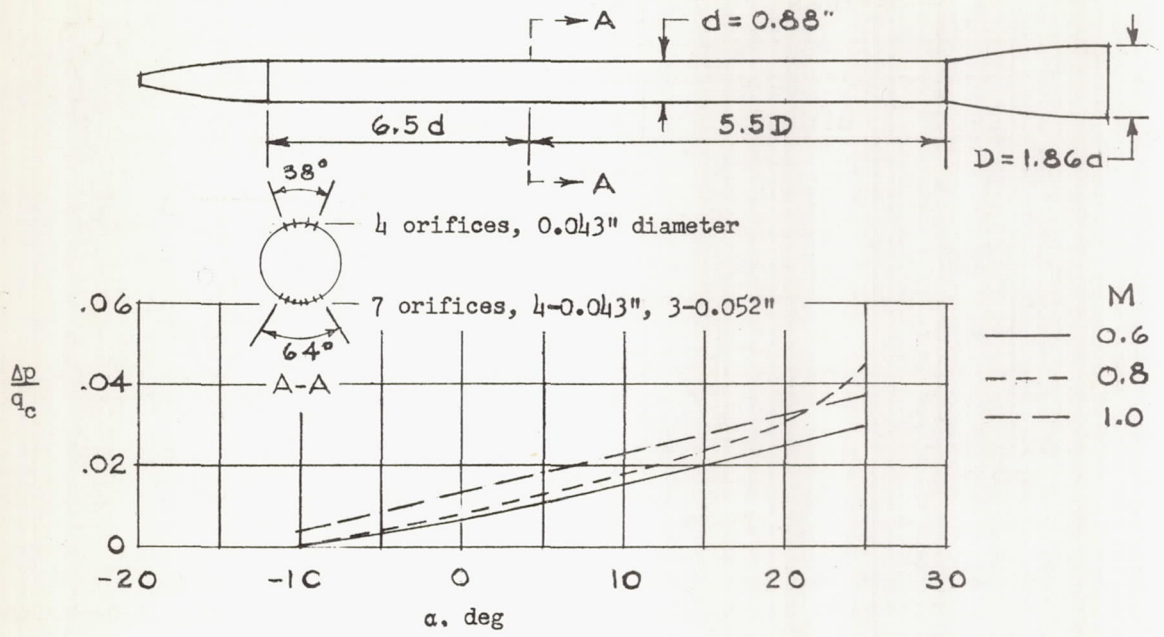


Figure 13.- Calibration at angles of attack of a static-pressure tube with an unsymmetrical orifice arrangement (ref. 18).

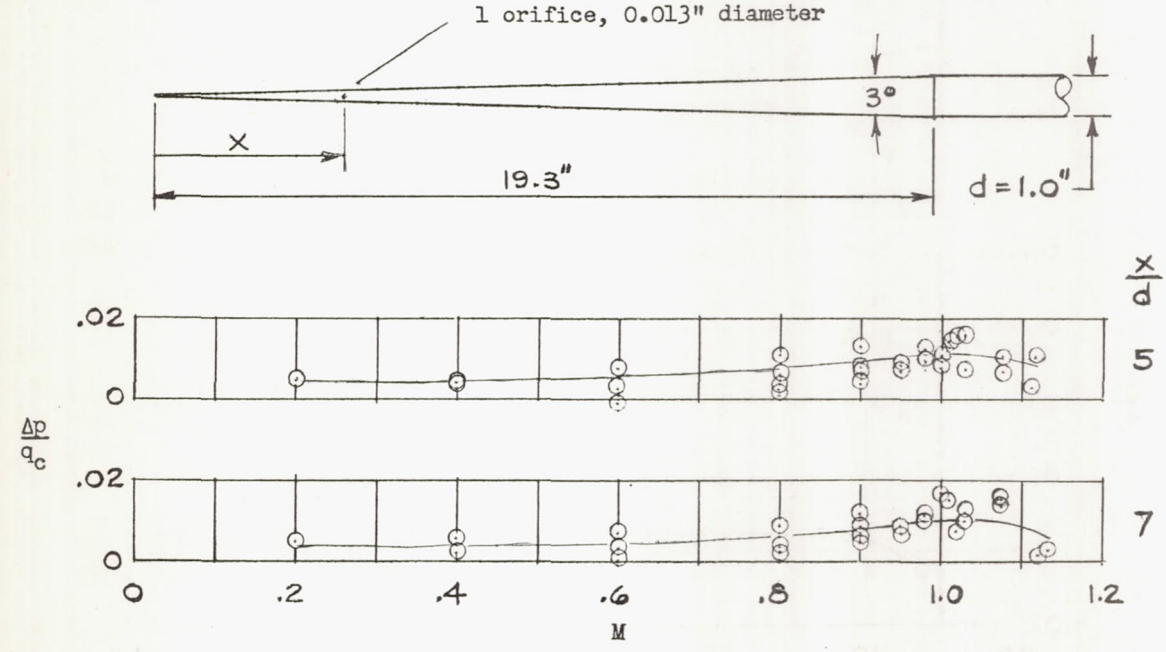


Figure 14.- Calibration of orifices on the nose section of a conical static-pressure tube at $\alpha = 1^{o}$ to $-1^{o}$.

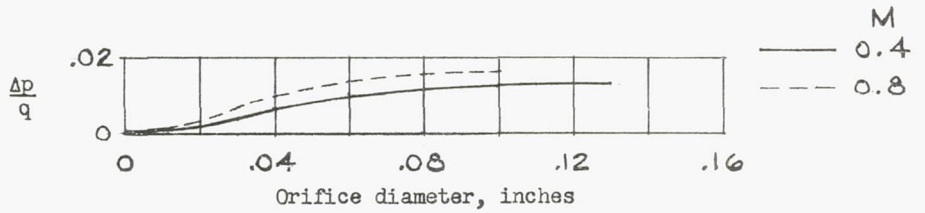


(a) Effect of orifice diameter (ref. 20).

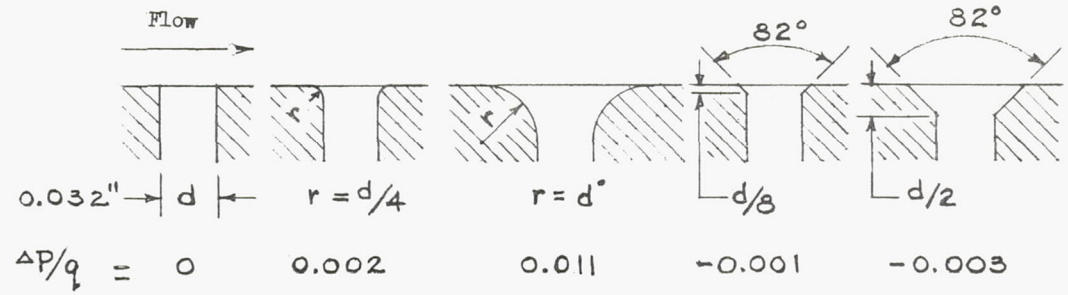


(b) Effect of edge shape of orifices. Static-pressure error of each edge shape referenced to square-edge orifice of 0.032-inch diameter (ref. 20).


(c) Effect of elongating orifices. Static-pressure error of slotted orifices referenced to 18-orifice configuration (ref. 21).

Figure 15.- Effect of orifice size and configuration on static-pressure measurements.

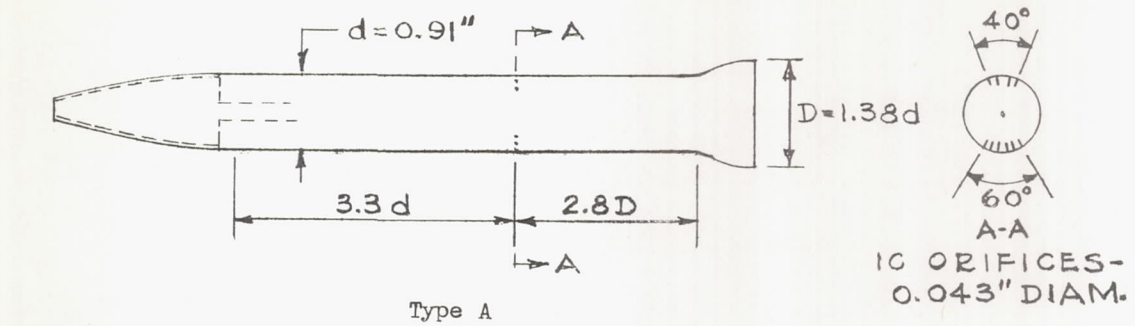


Type A

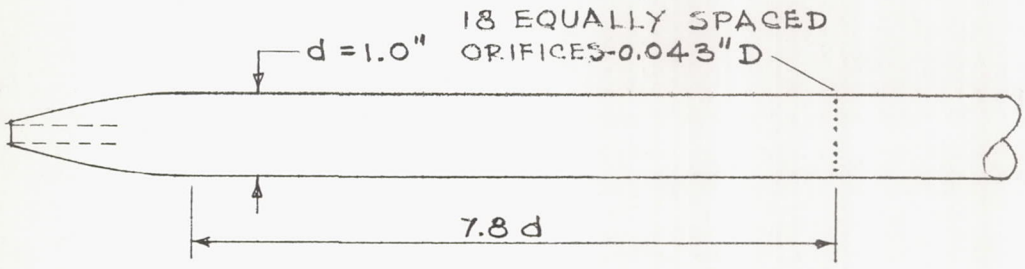


Type B

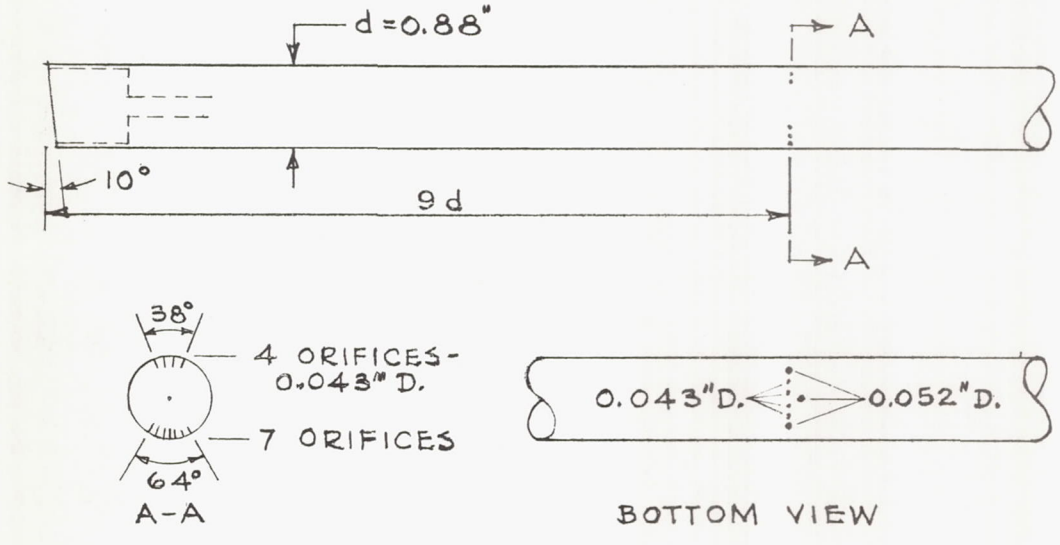


Type C

Figure 16.- Diagrams of static-pressure tubes used on airplane installations (1/2 scale).

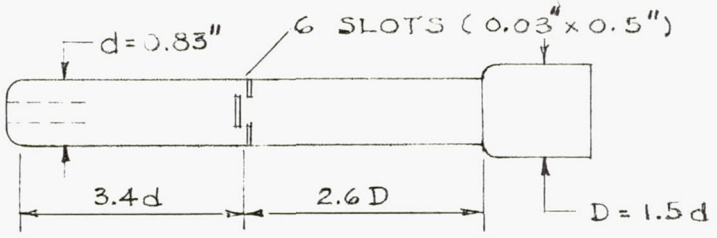


Type D

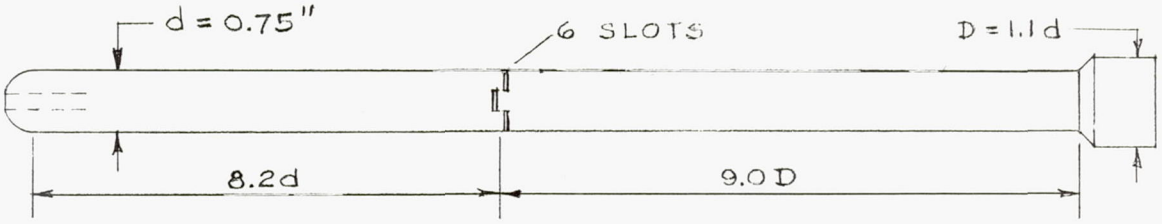


Type E

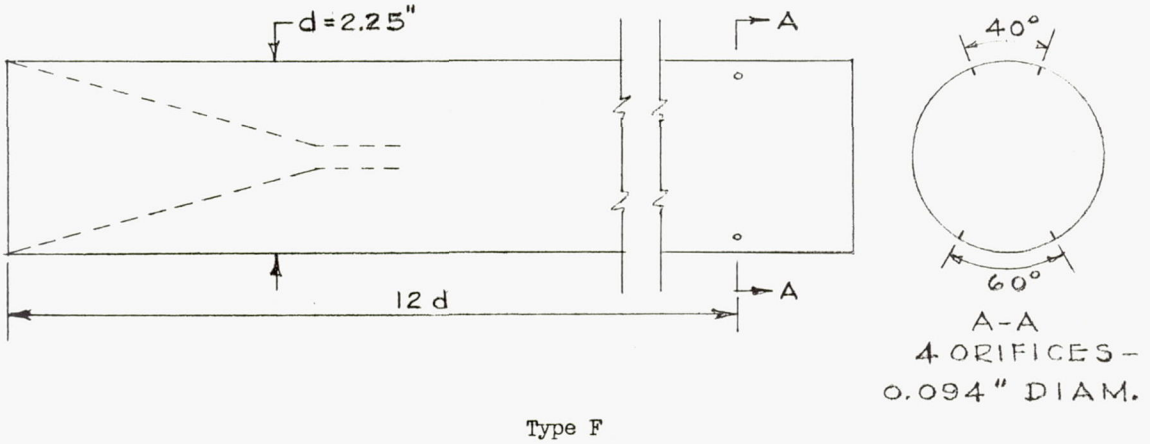


Type F

Figure 16.- Concluded.

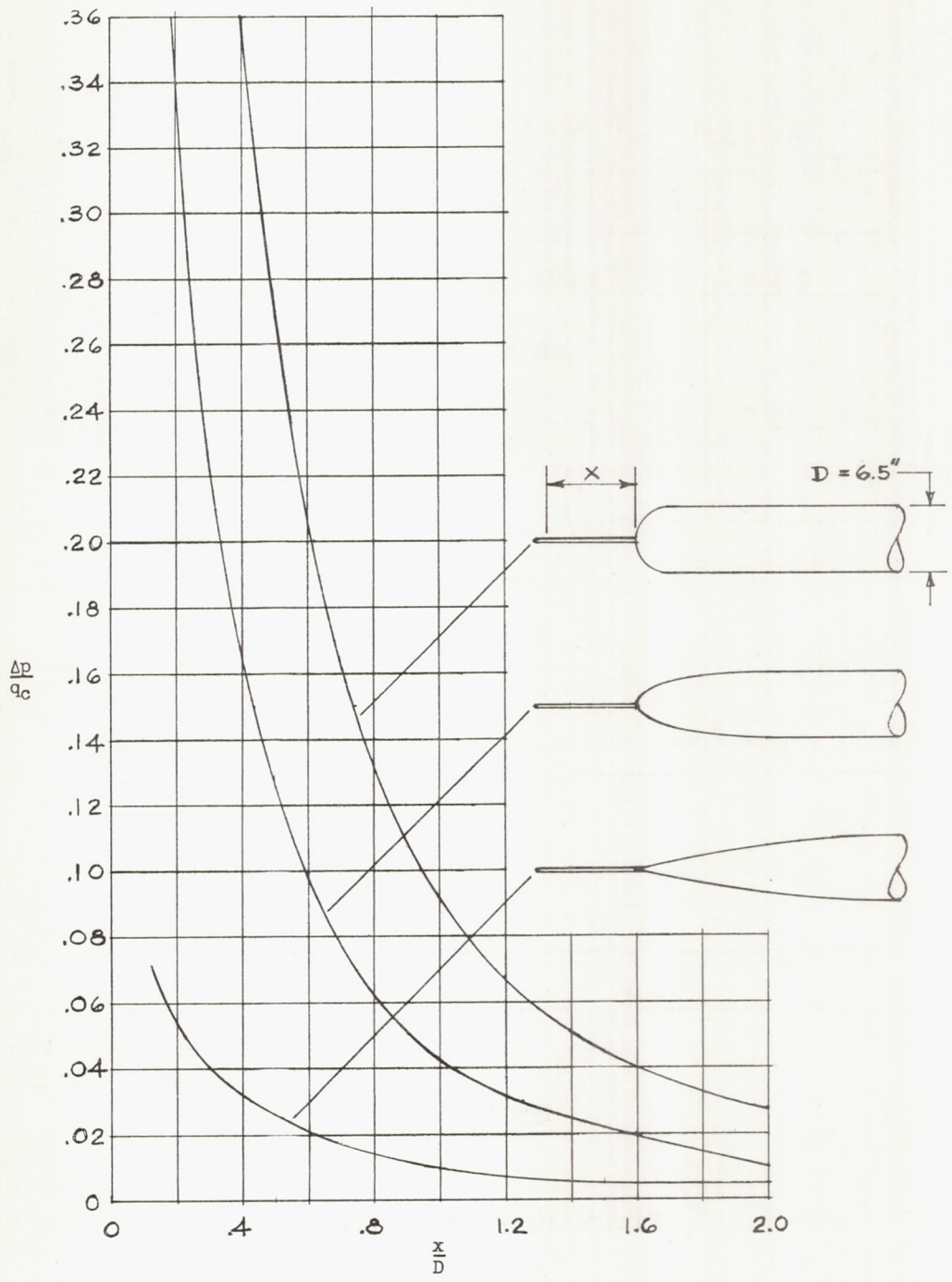


Figure 17.- Static-pressure errors at various distances ahead of three bodies of revolution with different nose shapes. M = 0.21; $\alpha = 0^{\circ}$ (ref. 22).

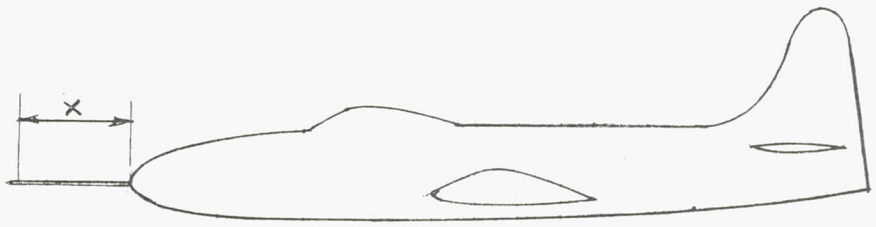


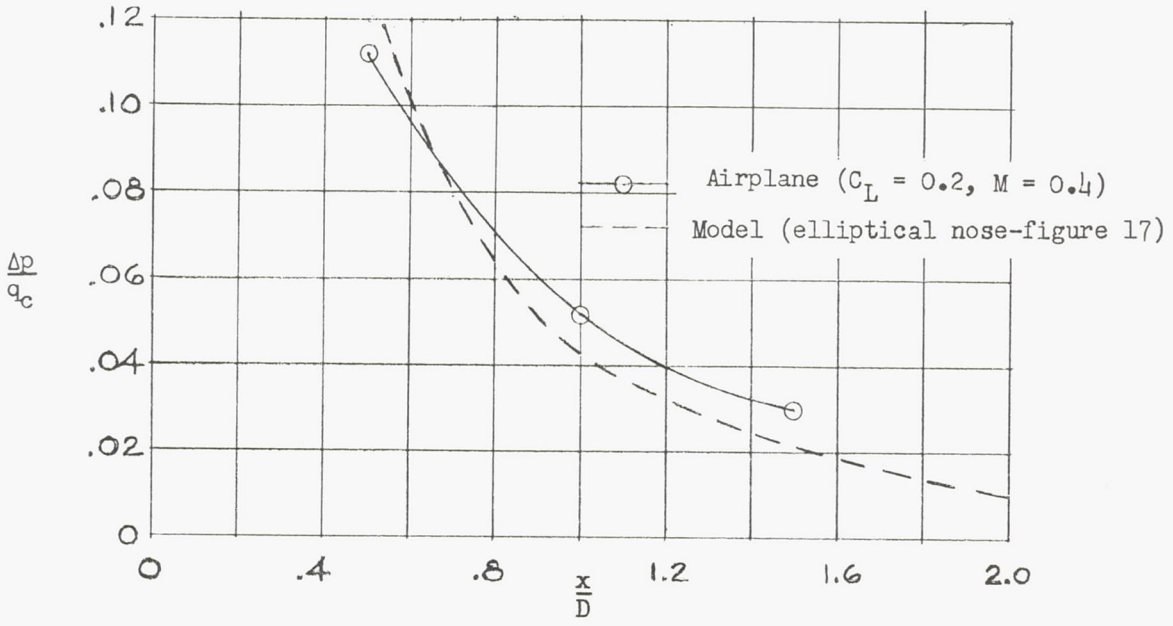


Variation of static-pressure error with distance ahead of the nose.

Figure 18.- Static-pressure errors at three distances ahead of an airplane fuselage with an elliptical nose shape (ref. 23).

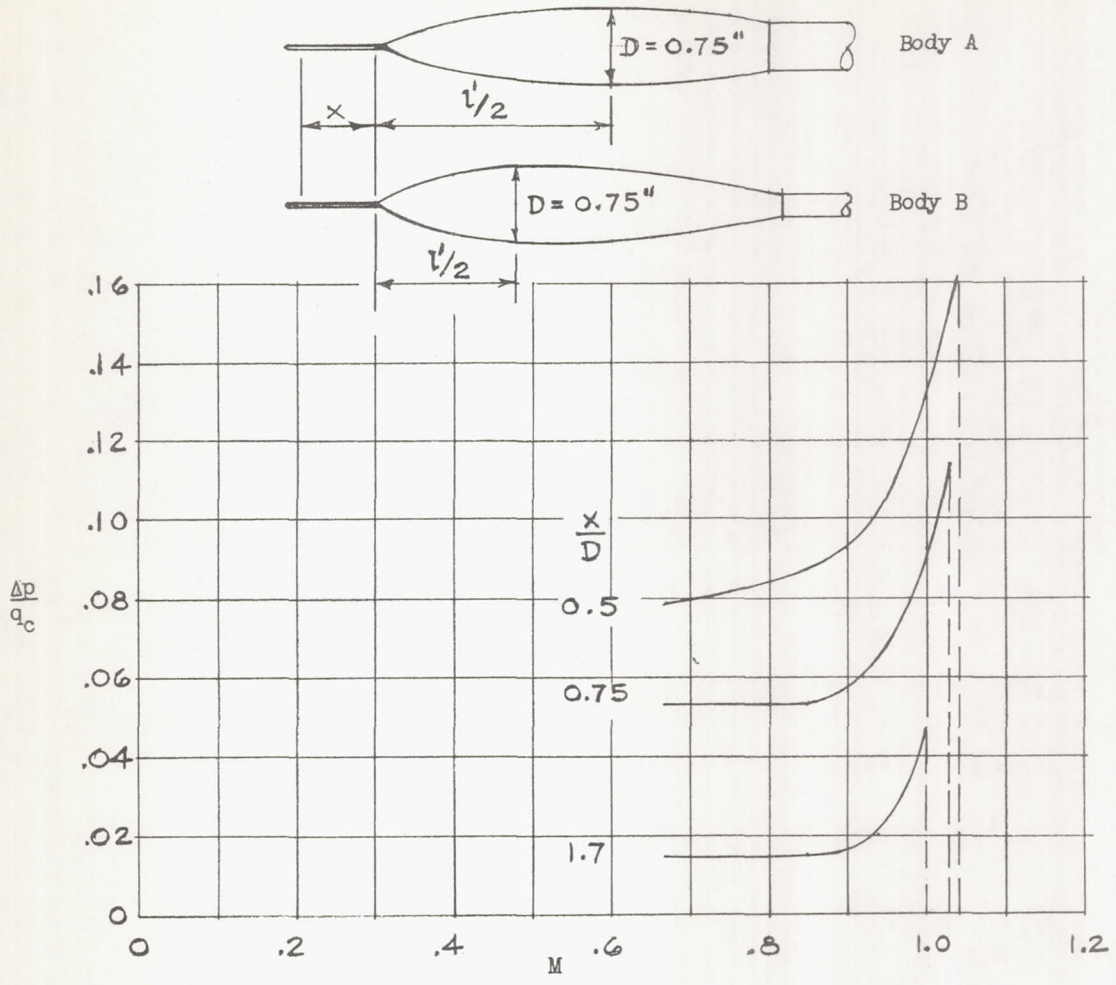


(a) Variation of static-pressure error with Mach number for body B.

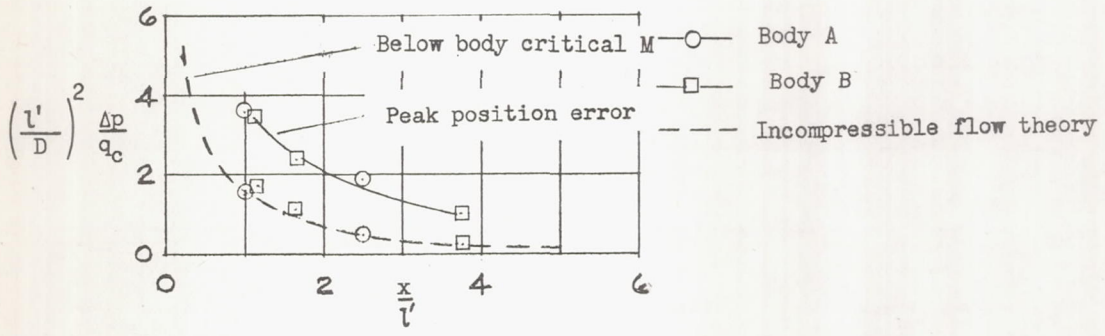


(b) Variation of static-pressure-error parameter with distance ahead of nose.

Figure 19.- Static-pressure errors at various distances ahead of two bodies of revolution at $\alpha = 0^{\circ}$ (ref. 24).

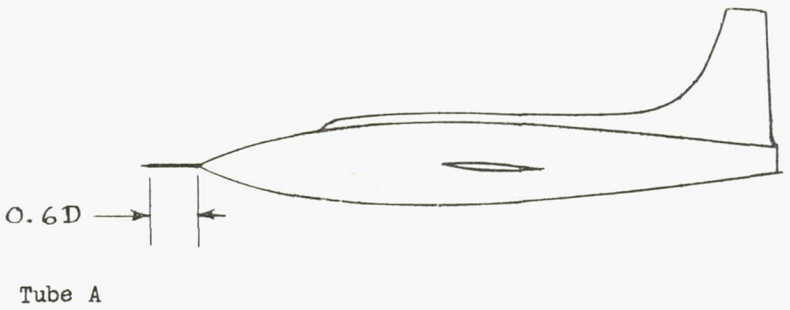


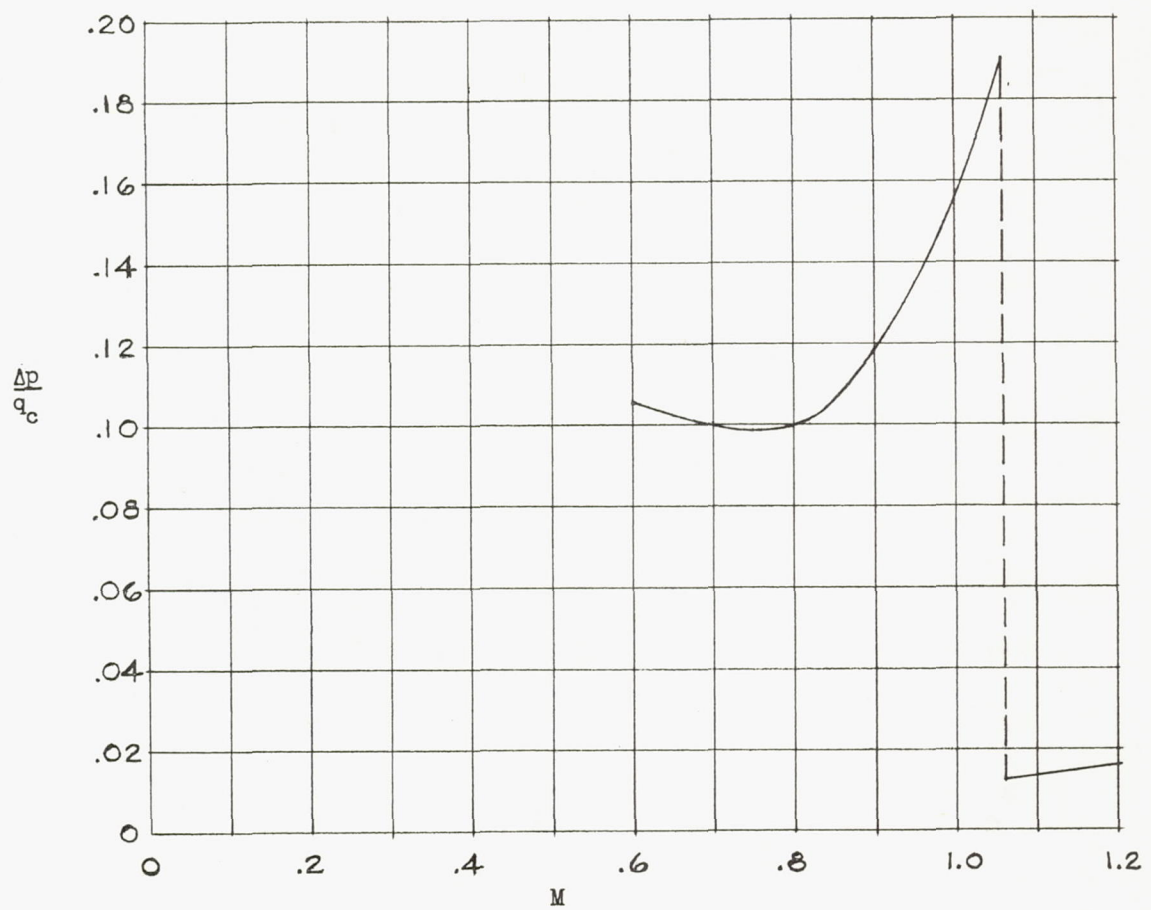


Figure 20.- Calibration in level flight of a static-pressure tube ahead of an airplane fuselage with a pointed nose (ref. 25).

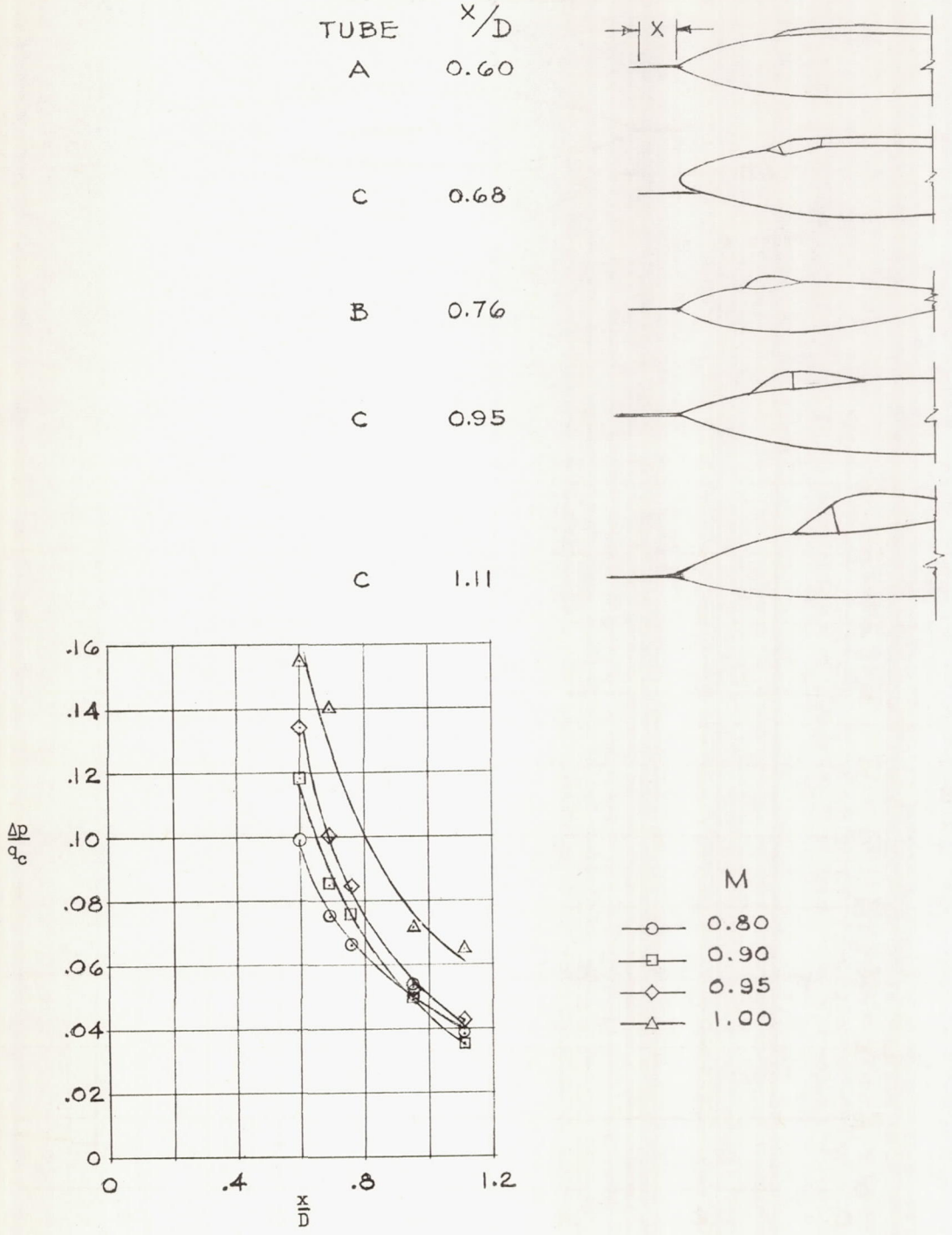


Figure 21.- Static-pressure errors ahead of five airplane fuselages with pointed noses (ref. 26).


Tube C

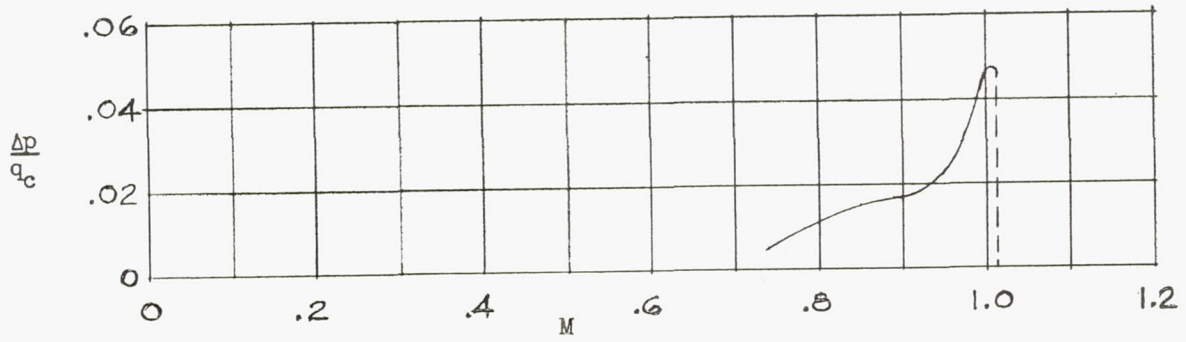


Figure 22.- Calibration in level flight of a static-pressure tube ahead of a fuselage with an elongated pointed nose (ref. 26).

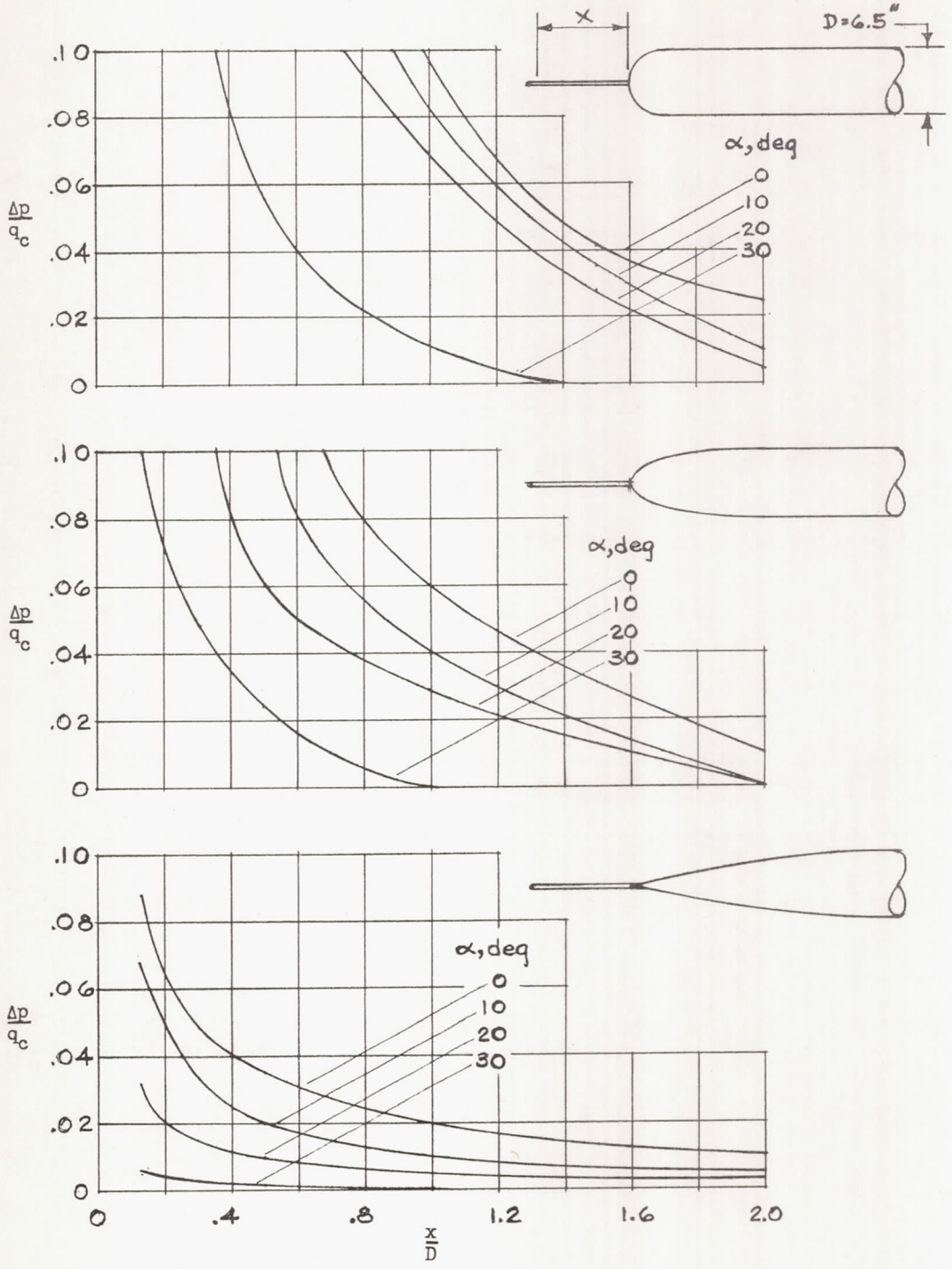


Figure 23.- Effect of angle of attack on the pressures at various distances ahead of three bodies of revolution with different nose shapes, M = 0.16 (ref. 22).

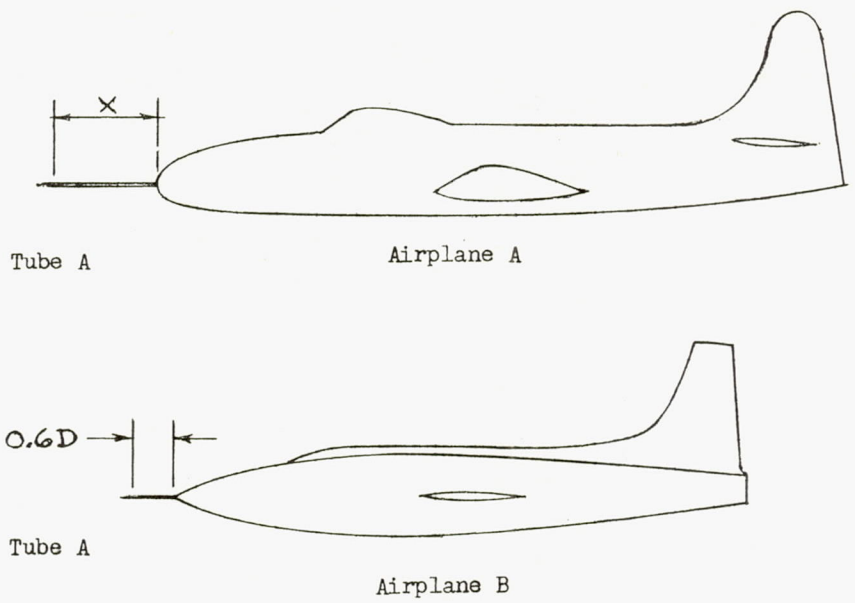


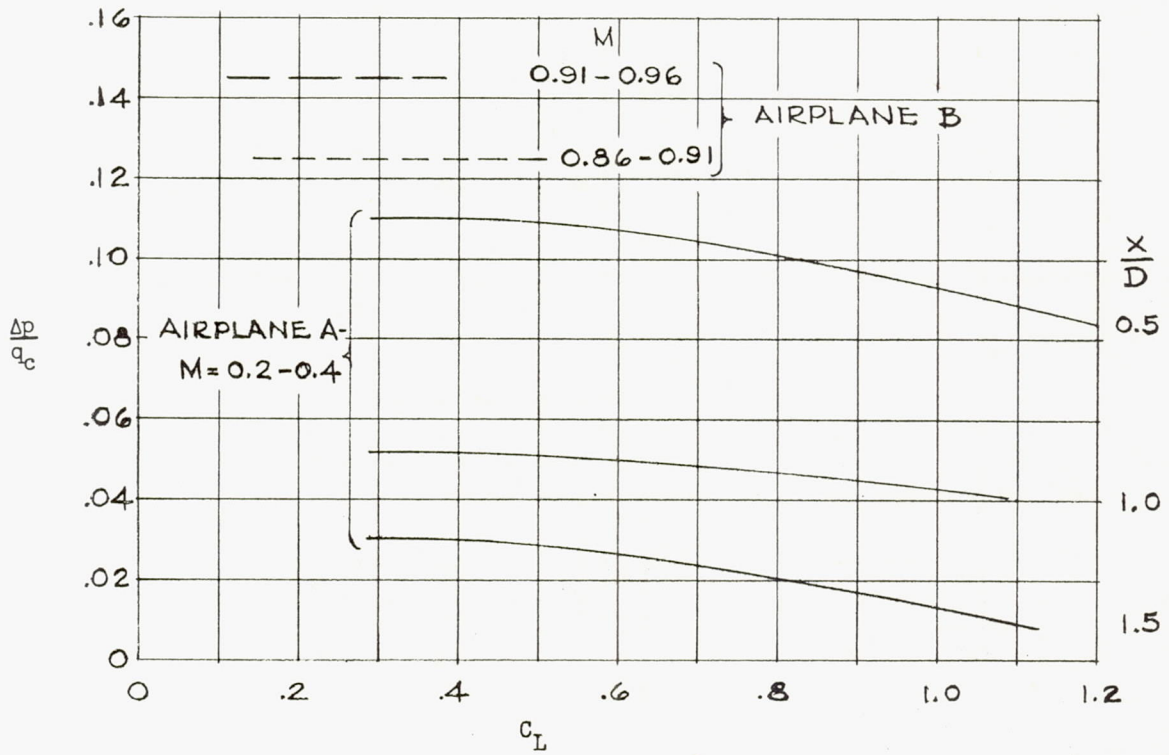


Figure 24.- Variation of static-pressure error with lift coefficient of fuselage-nose installations on two airplanes (refs. 23 and 25).

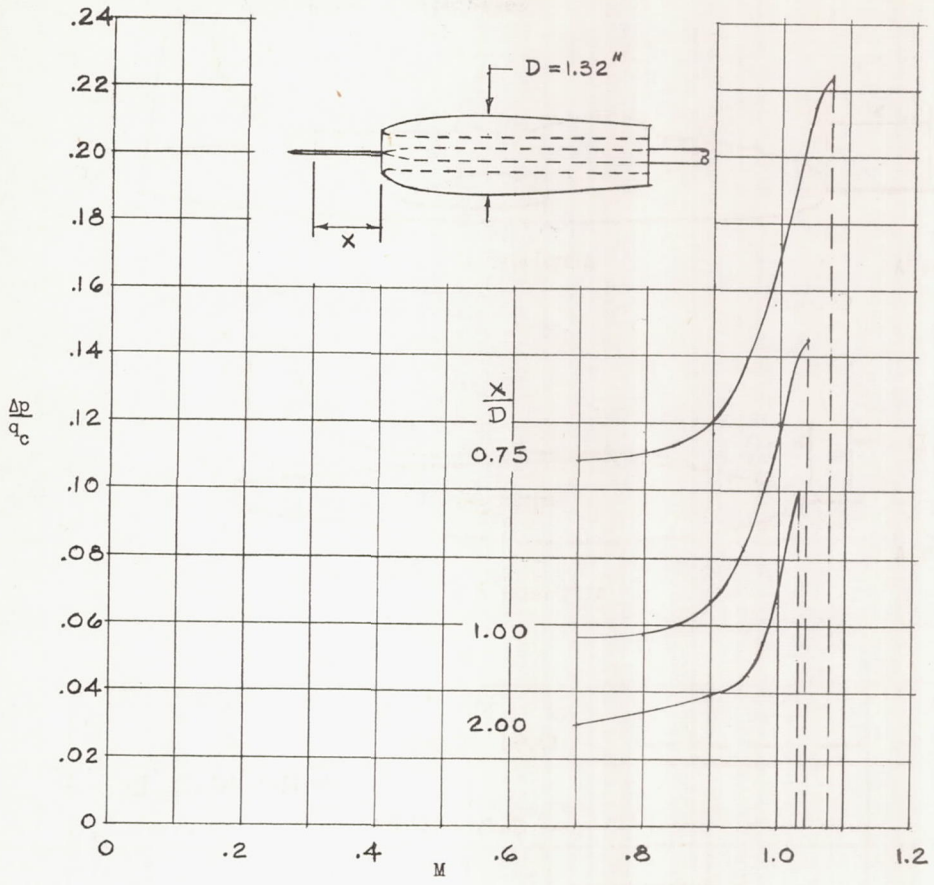


(a) Variation of static-pressure error with Mach number (inlet-velocity ratio 0.68 at M = 0.7; 0.57 at M = 1.0).

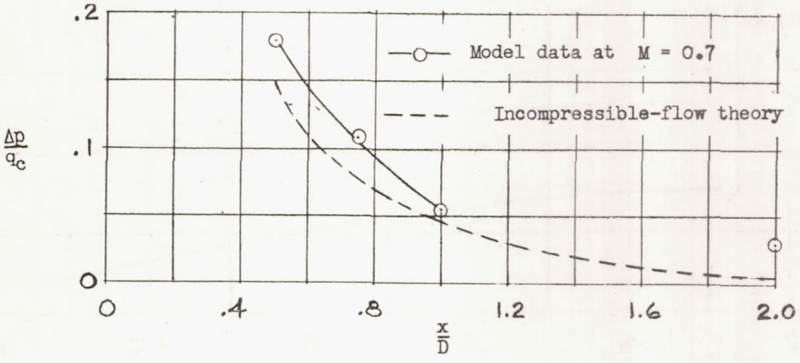


(b) Variation of static-pressure error with distance ahead of nose.

Figure 25.- Static-pressure errors at three distances ahead of a body of revolution with a nose inlet (ref. 24).


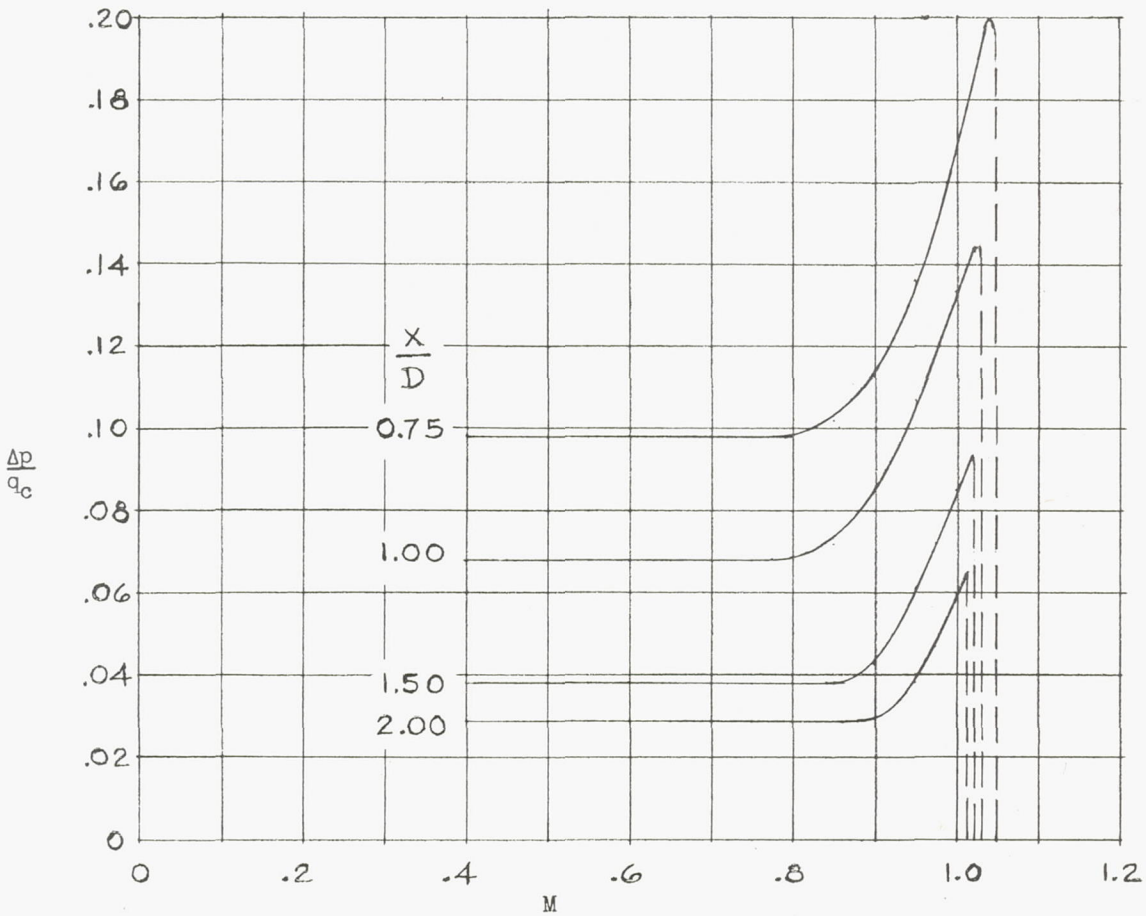


Figure 26.- Calibration in level flight of static-pressure orifices at four distances ahead of an airplane fuselage with a nose inlet (ref. 28).

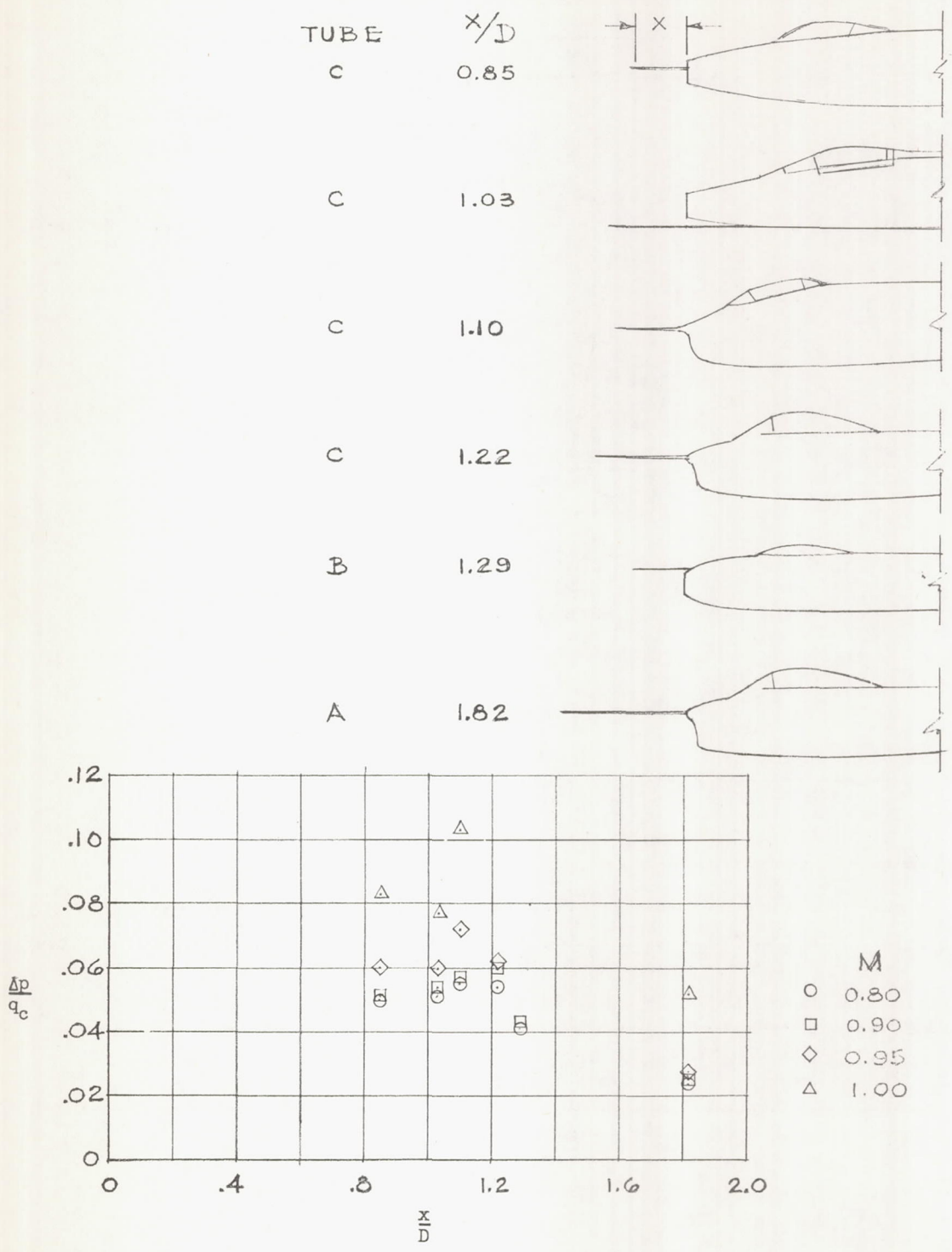


Figure 27.- Static-pressure errors ahead of six airplane fuselages with nose inlets (ref. 26).

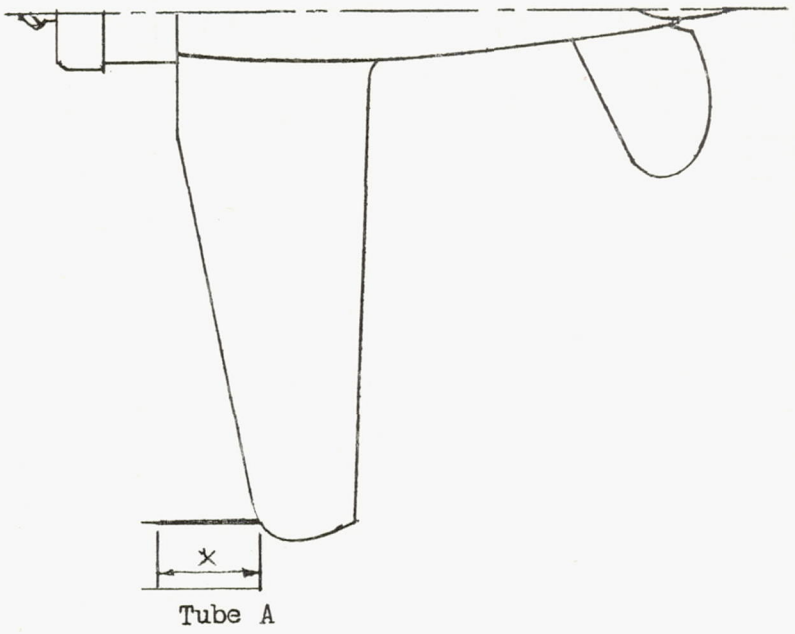


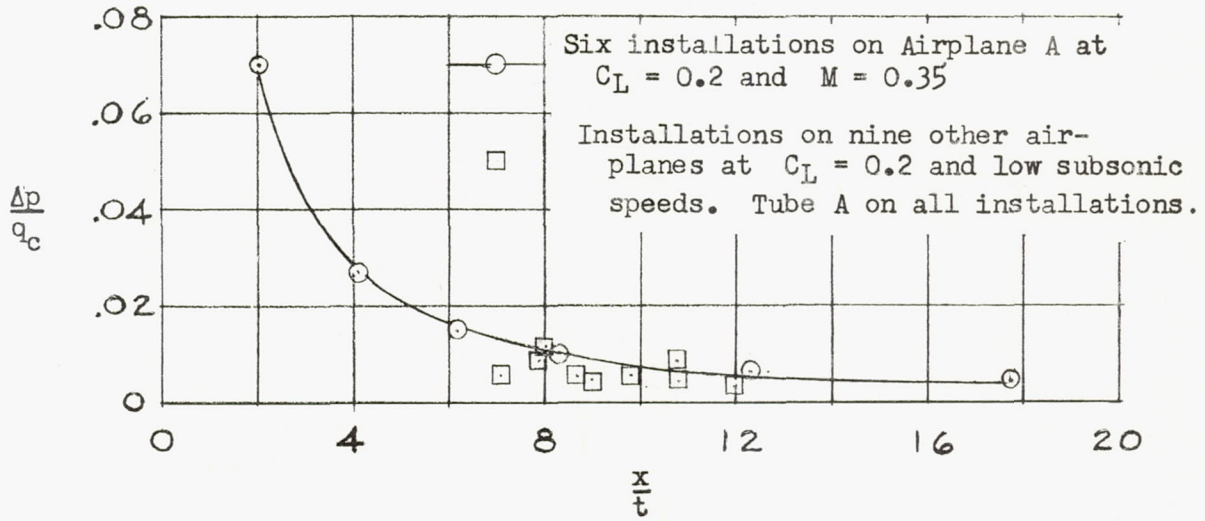


Figure 28.- Static-pressure errors at various distances ahead of the wing tips of unswept-wing airplanes (ref. 23).

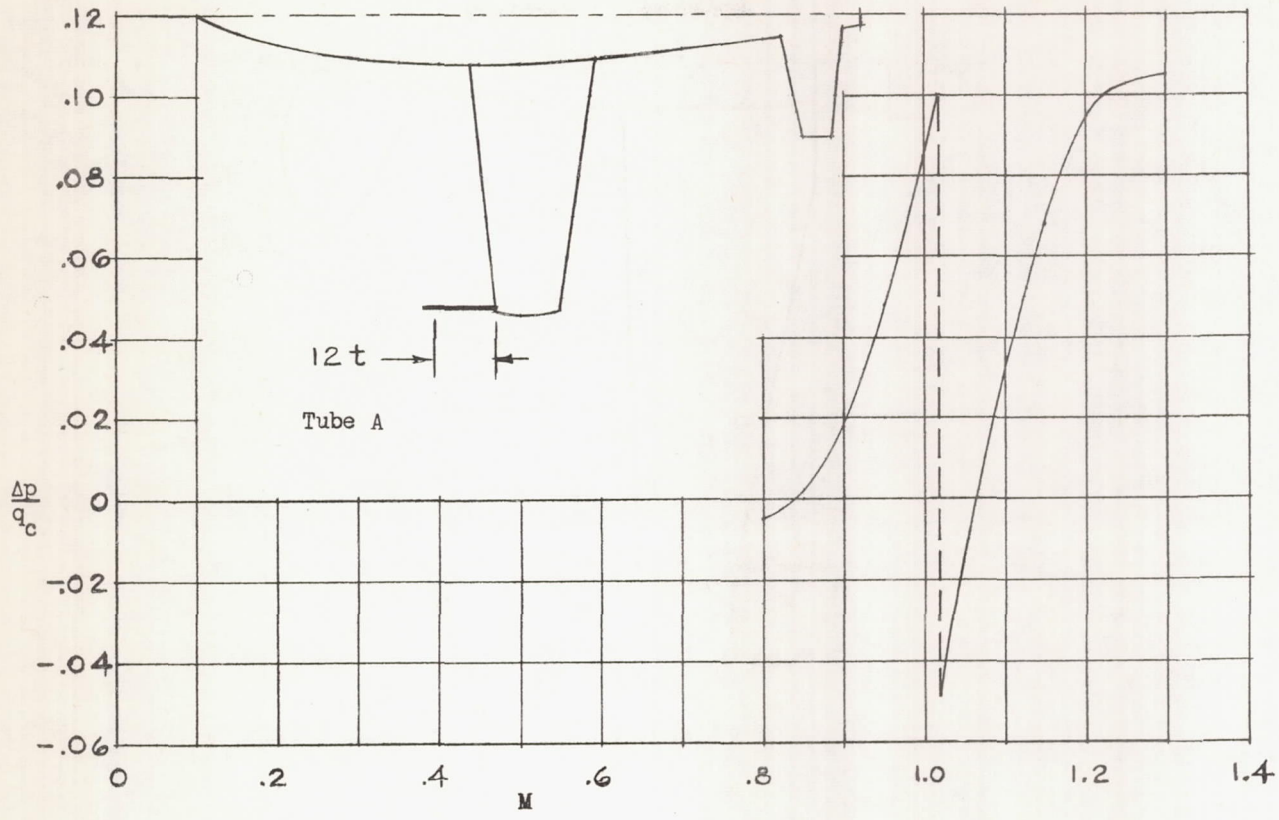


Figure 29.- Calibration in level flight of a static-pressure tube ahead of the wing tip of an unswept-wing airplane (ref. 25).

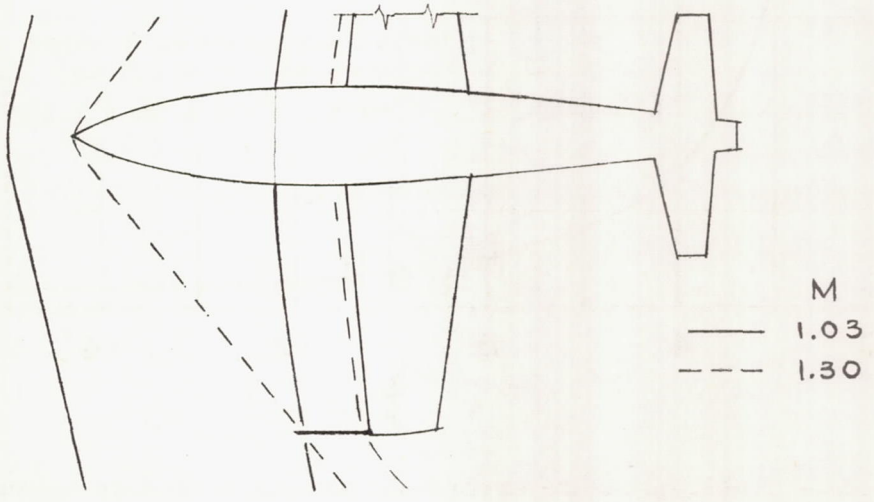


Figure 30.- Diagram showing position of shock waves with respect to a wing-tip installation on an unswept-wing airplane.

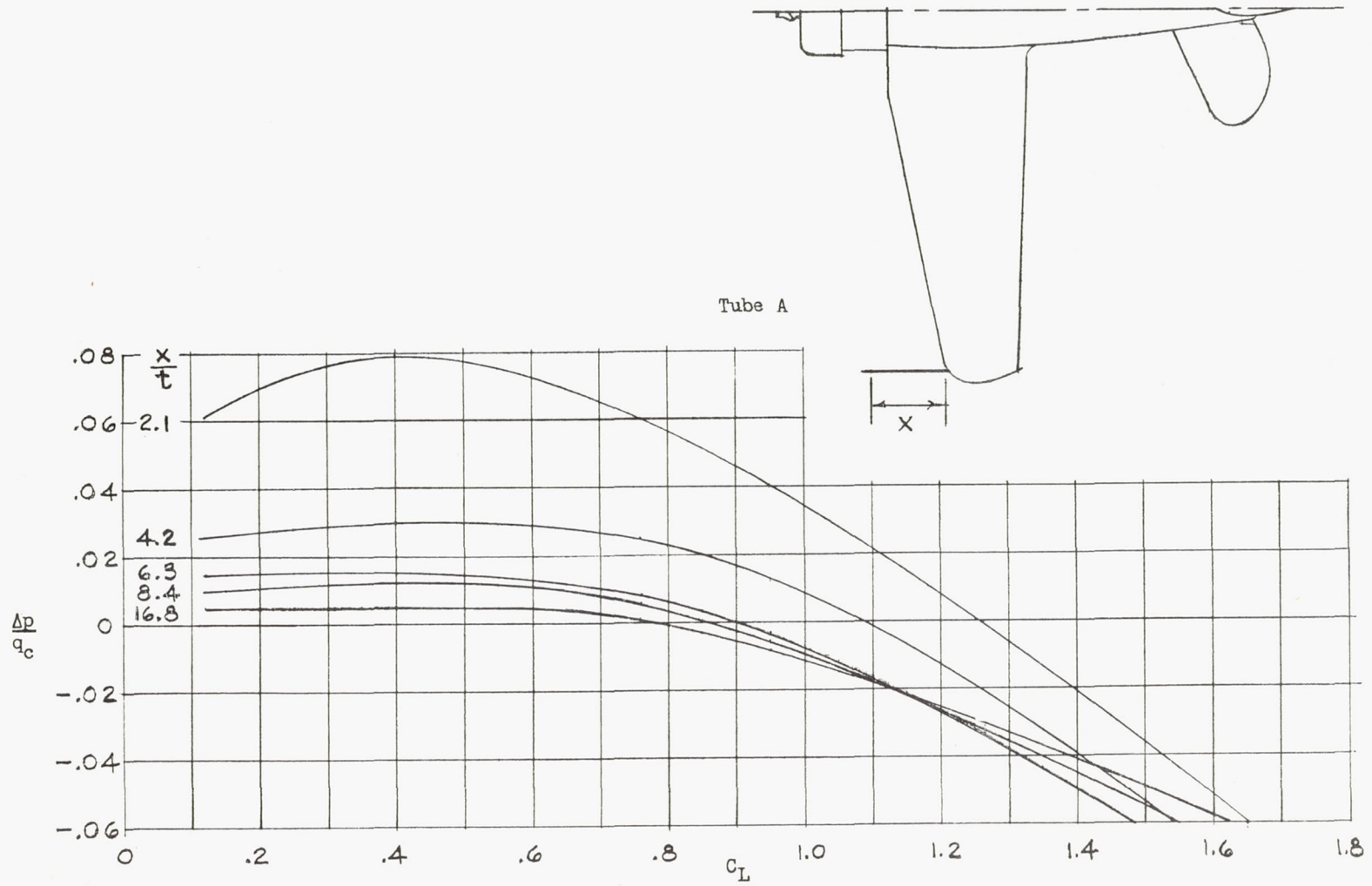


Figure 31.- Variation of static-pressure error with lift coefficient at five distances ahead of the wing tip of an unswept-wing airplane. M = 0.1 to 0.36 (ref. 23).

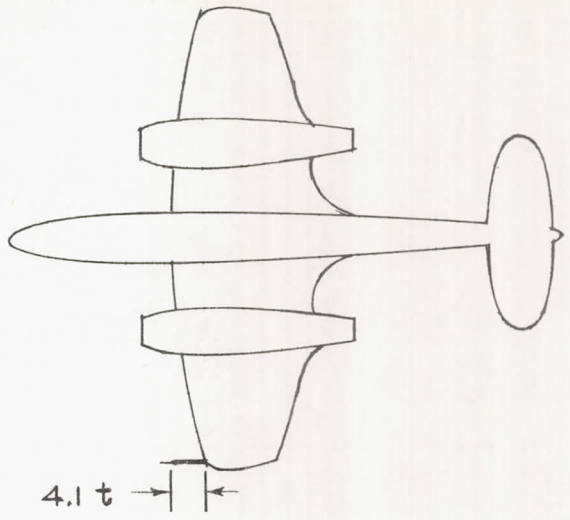


Tube D

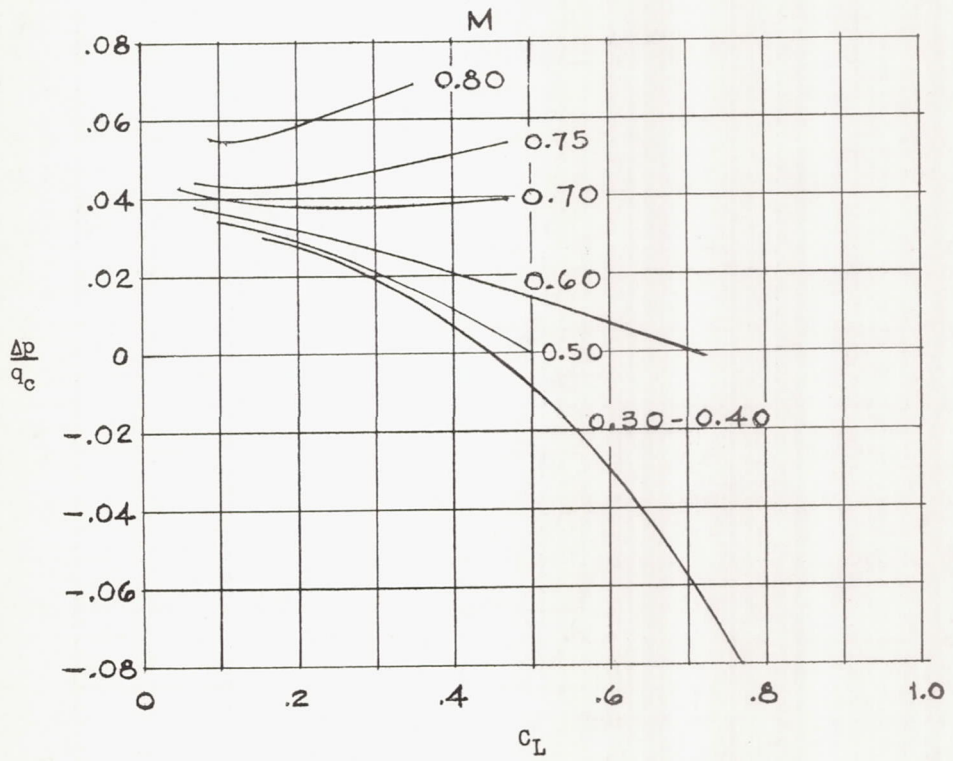


Figure 32.- Variation of static-pressure error with lift coefficient for a wing-tip installation on an unswept-wing airplane (ref. 29).

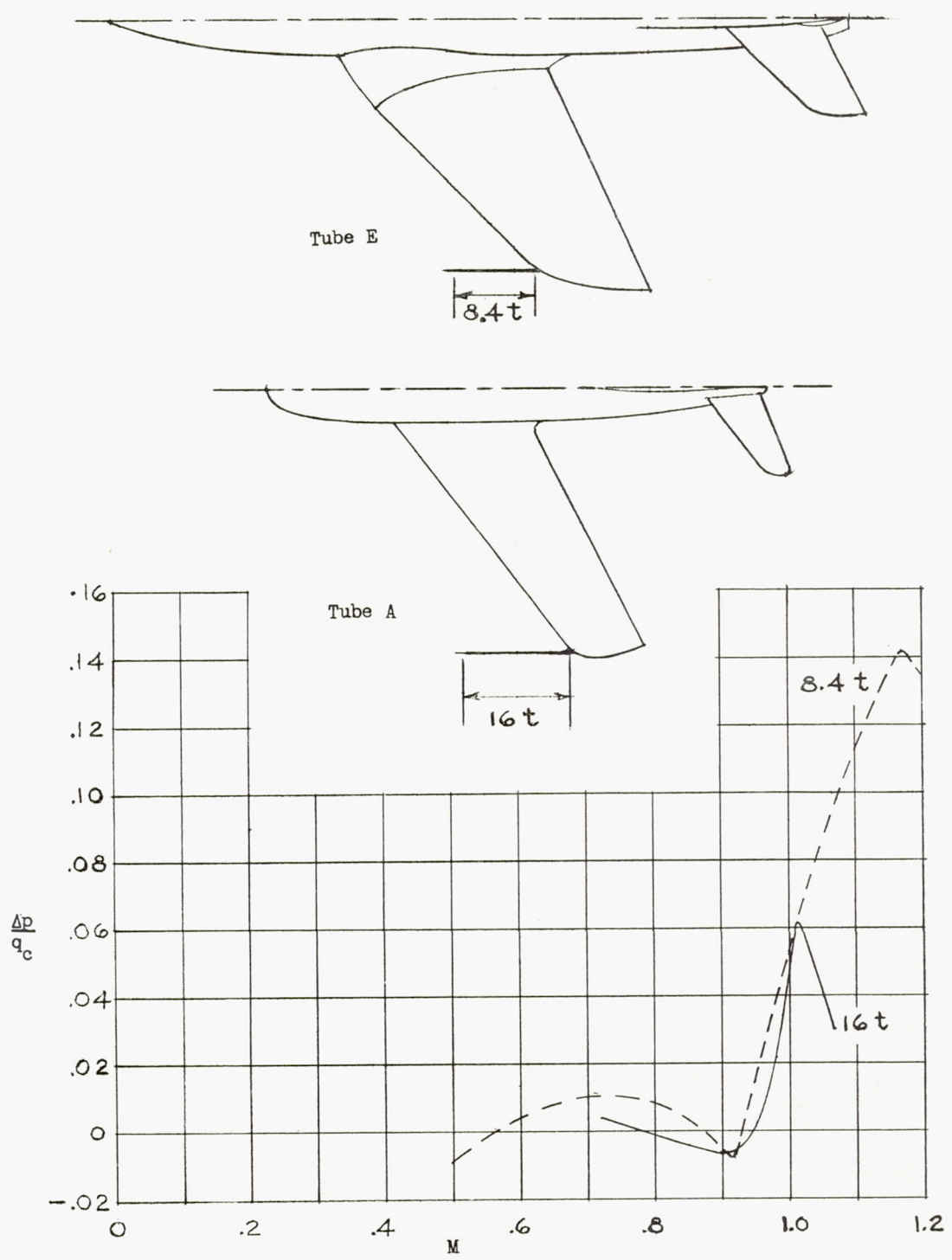


Figure 33.- Calibration in level flight of wing-tip installations on two swept-wing airplanes (refs. 30 and 31).

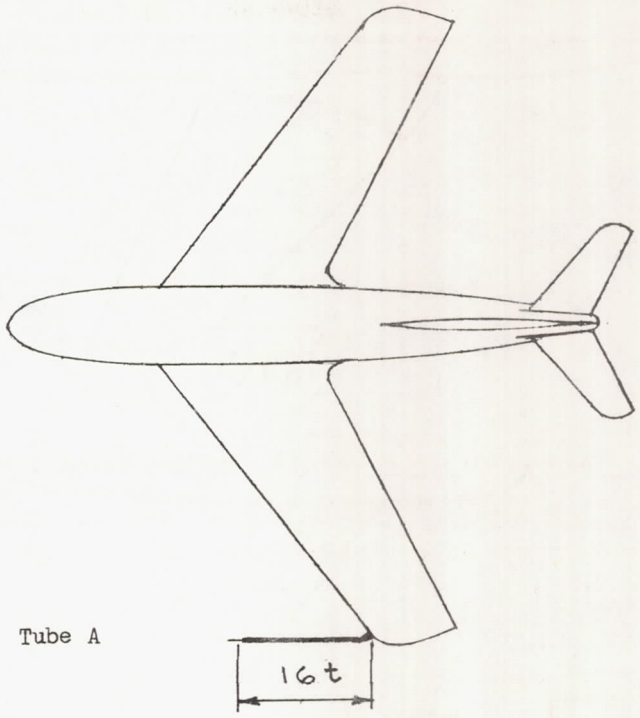


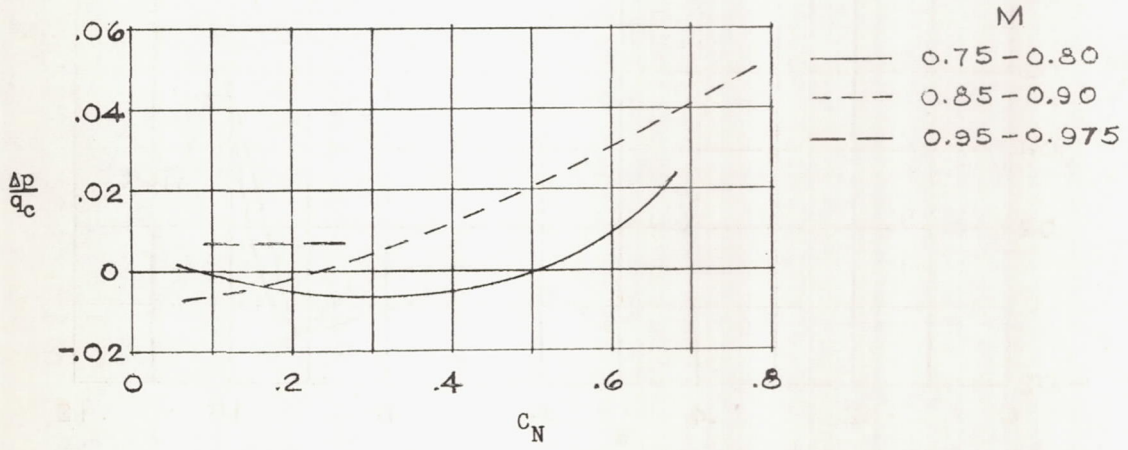


Figure 34.- Variation of static-pressure error with normal-force coefficient for a wing-tip installation on a swept-wing airplane (ref. 30).

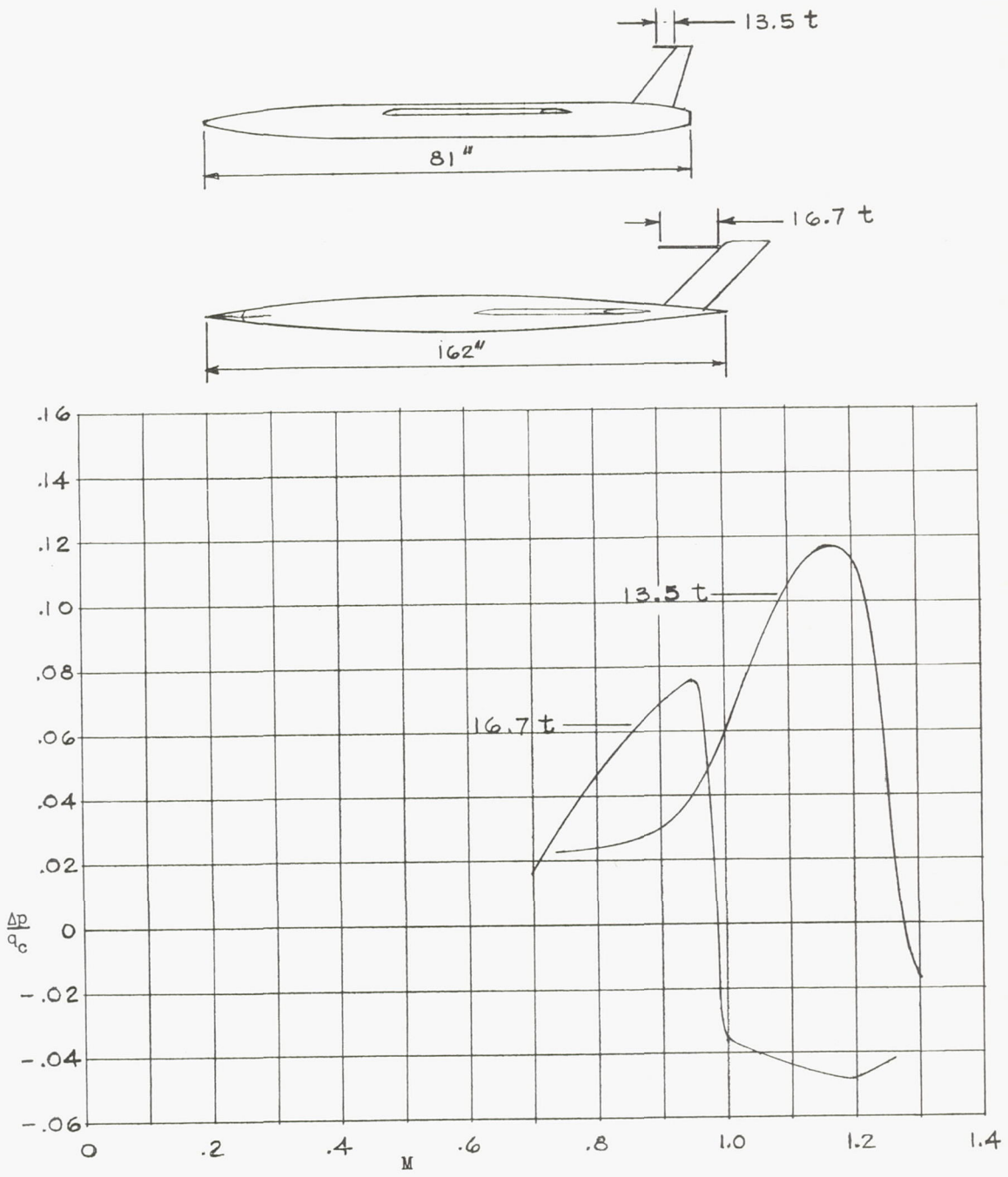


Figure 35.- Calibrations of vertical-tail-fin installations on free-flight models.

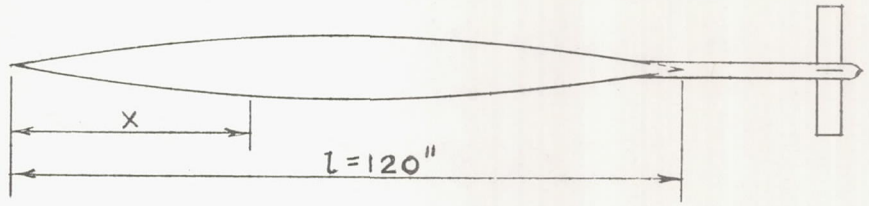


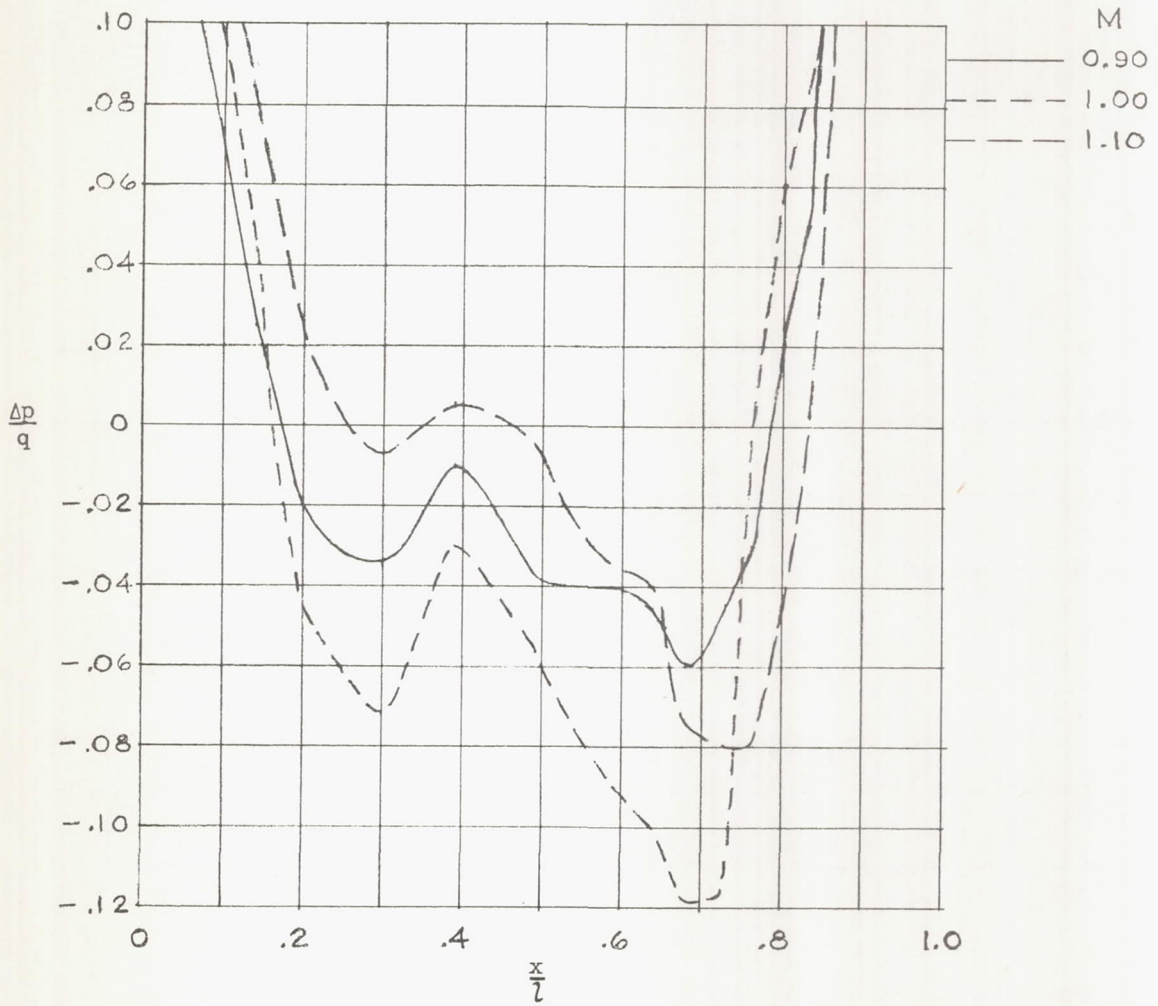


Figure 36.- Pressure distribution along a body of revolution at $\alpha = 0^{\circ}$ (ref. 34).

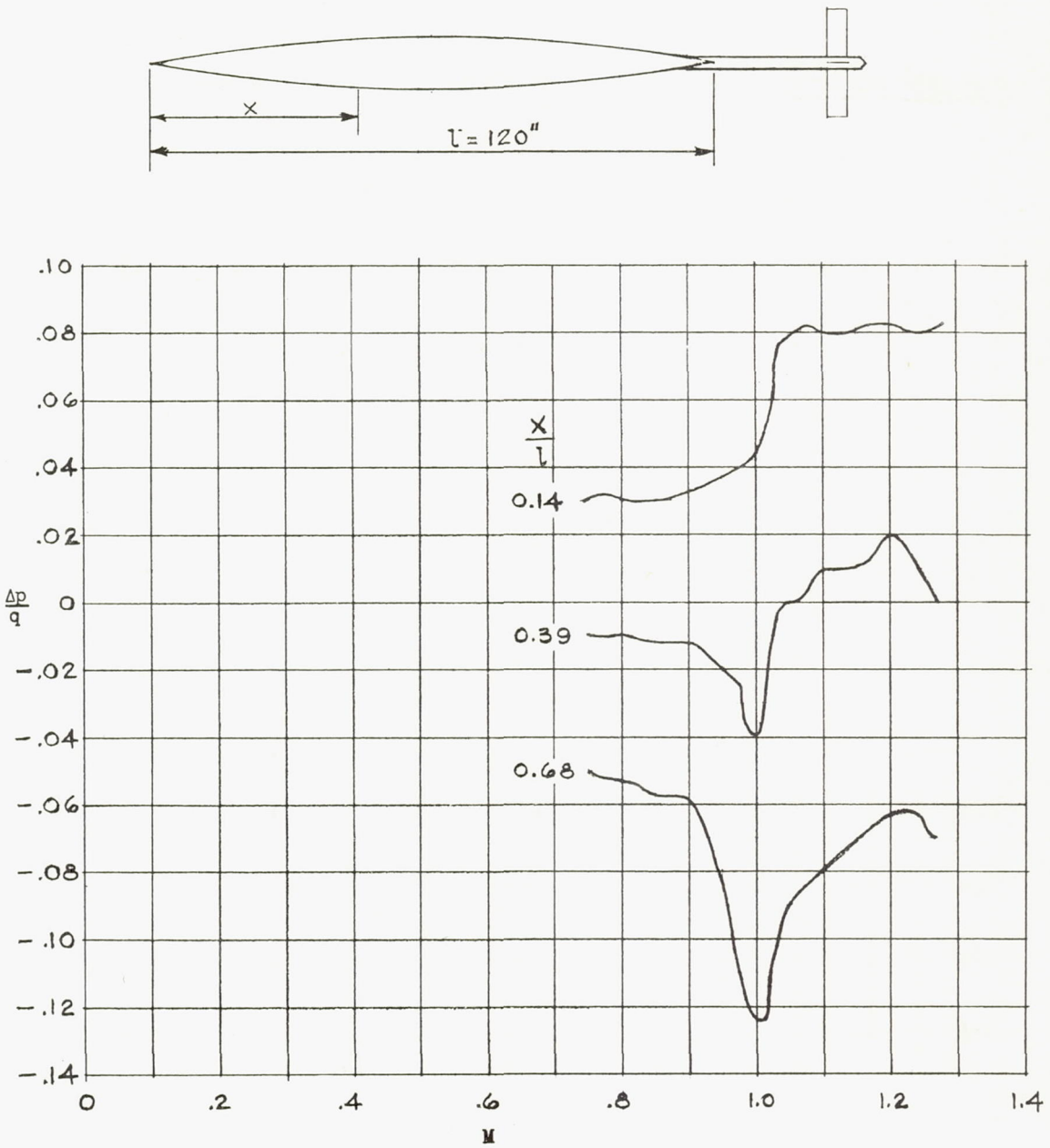


Figure 37.- Calibrations of orifices at three positions along a body of revolution at $\alpha = 0^{\circ}$ (ref. 34).

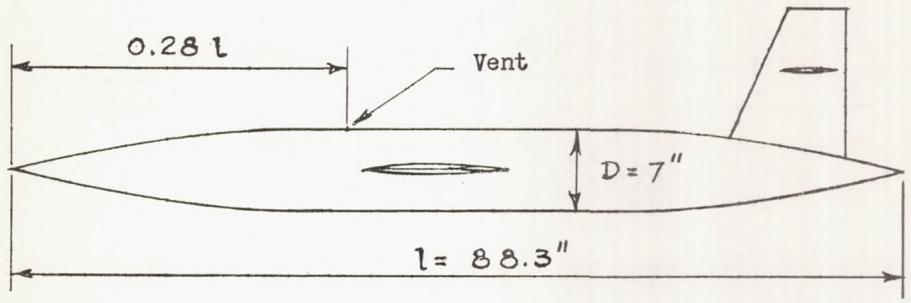


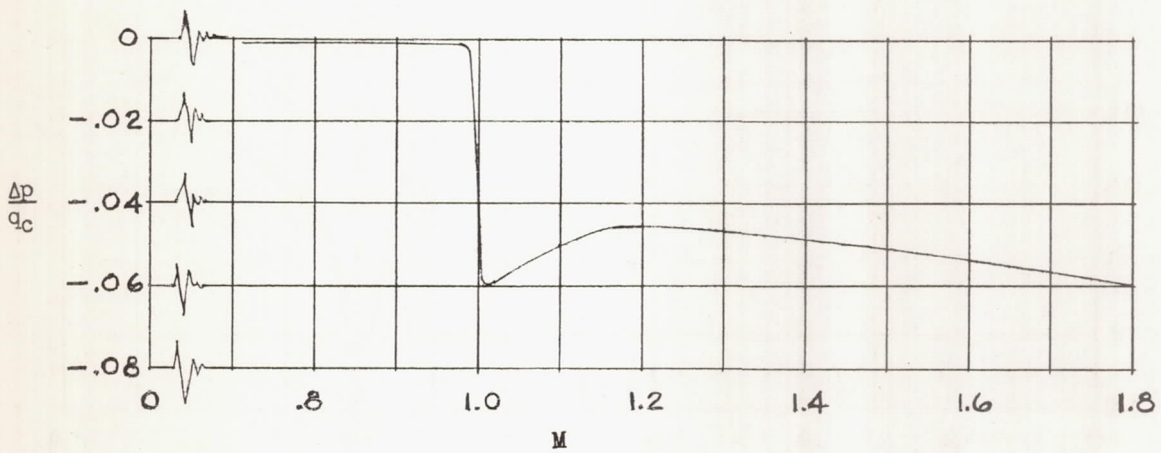


Figure 38.- Calibration of an orifice on a free-flight model.

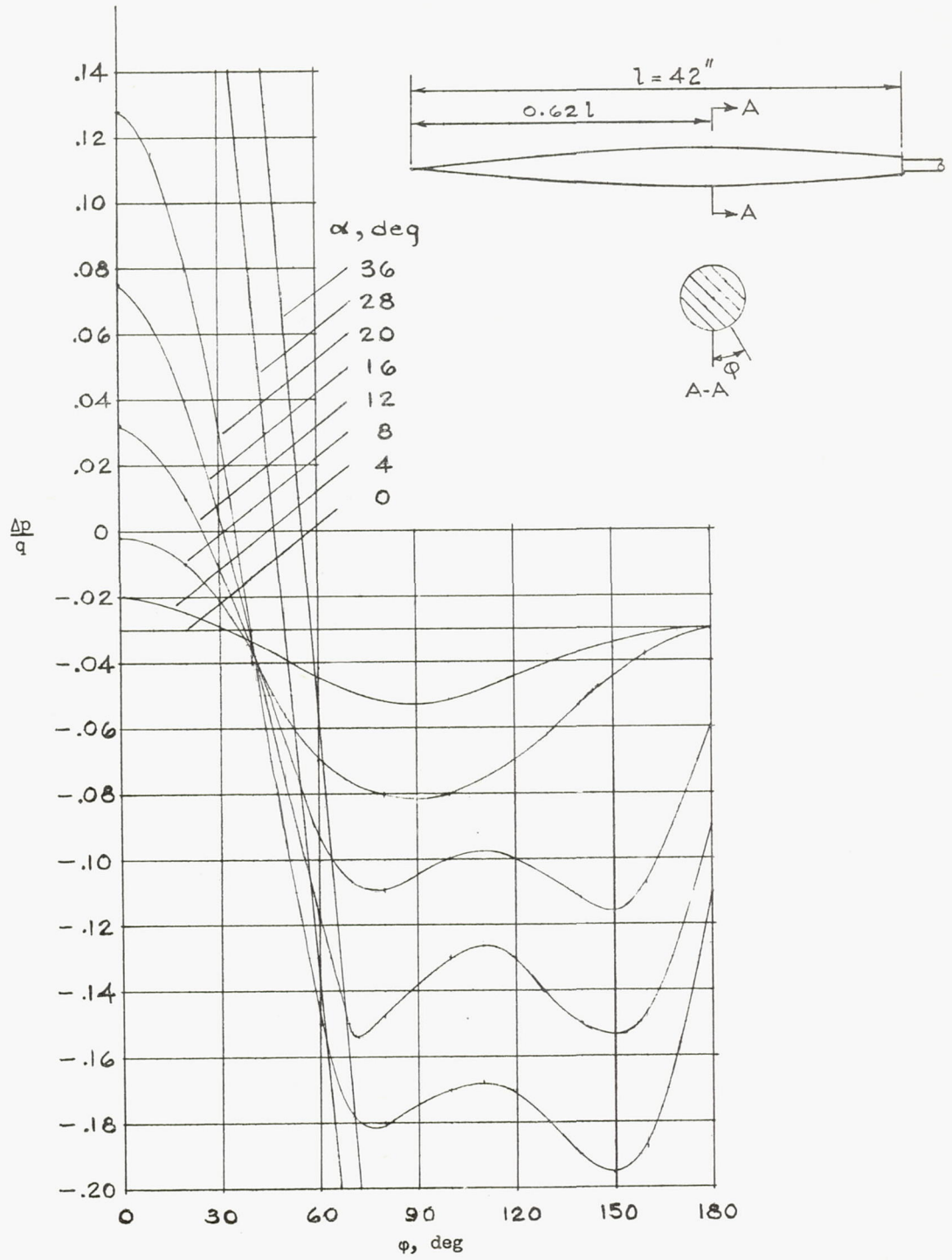


Figure 39.- Variation of the circumferential pressure distribution with angle of attack at the maximum diameter of a body of revolution at M = 1.59 (ref. 37).

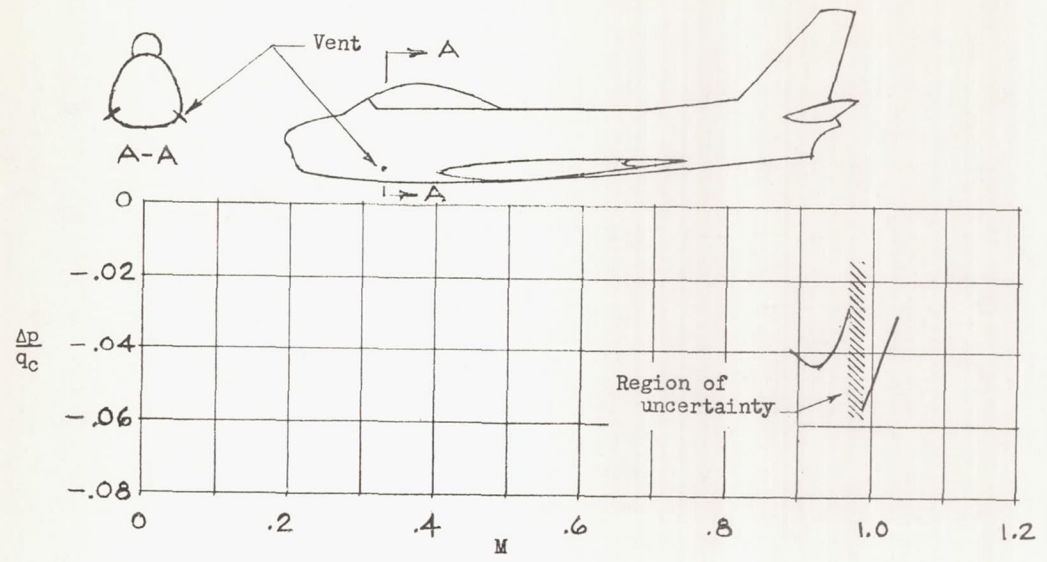


(a) Variation of static-pressure error with Mach number.

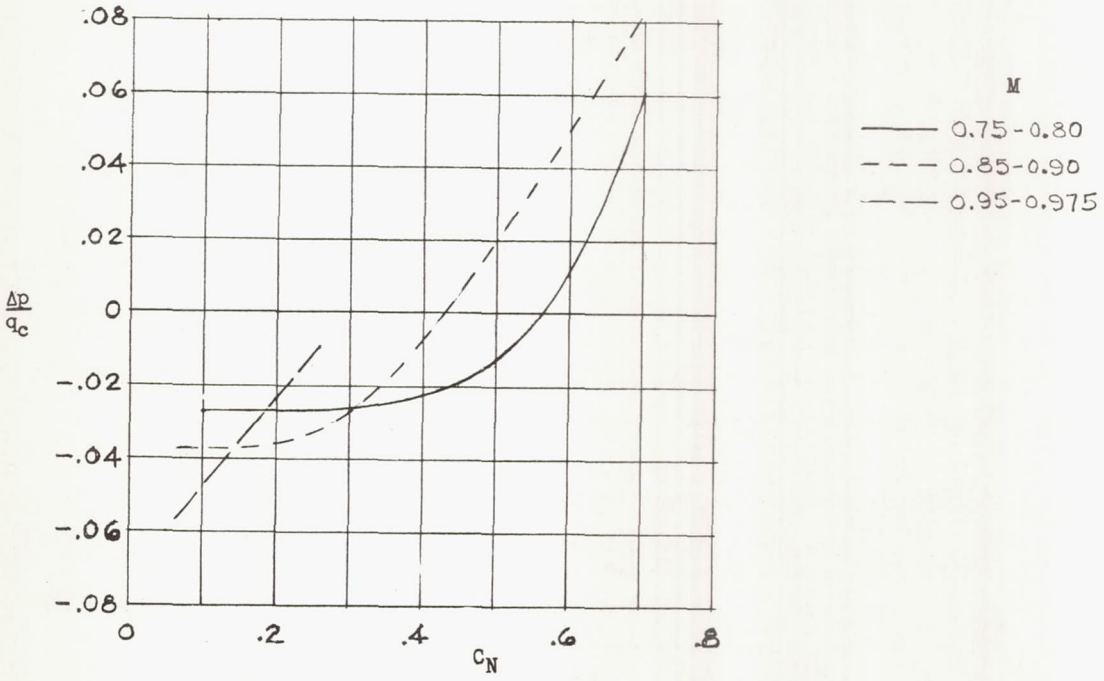


(b) Variation of static-pressure error with normal-force coefficient.

Figure 40.- Calibration of a static-pressure vent on an airplane fuselage (ref. 30).

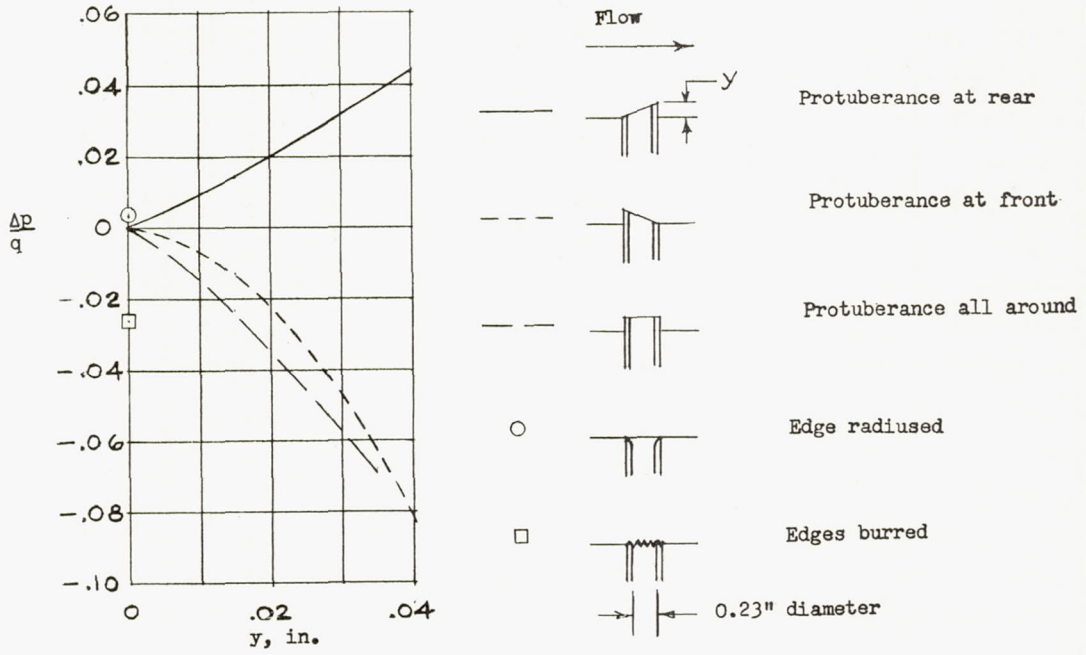


(a) Effect of protuberances and indentations.

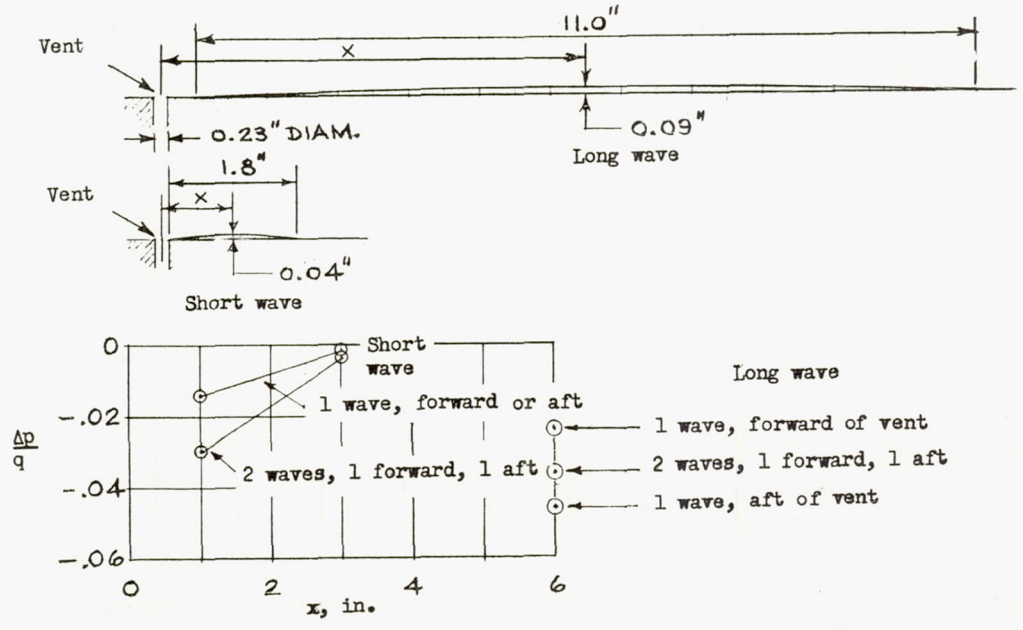


(b) Effect of waviness of skin in vicinity of vent.

Figure 41.- Variation of static-pressure error with configuration of static-pressure vents at a speed of 175 knots (ref. 38).

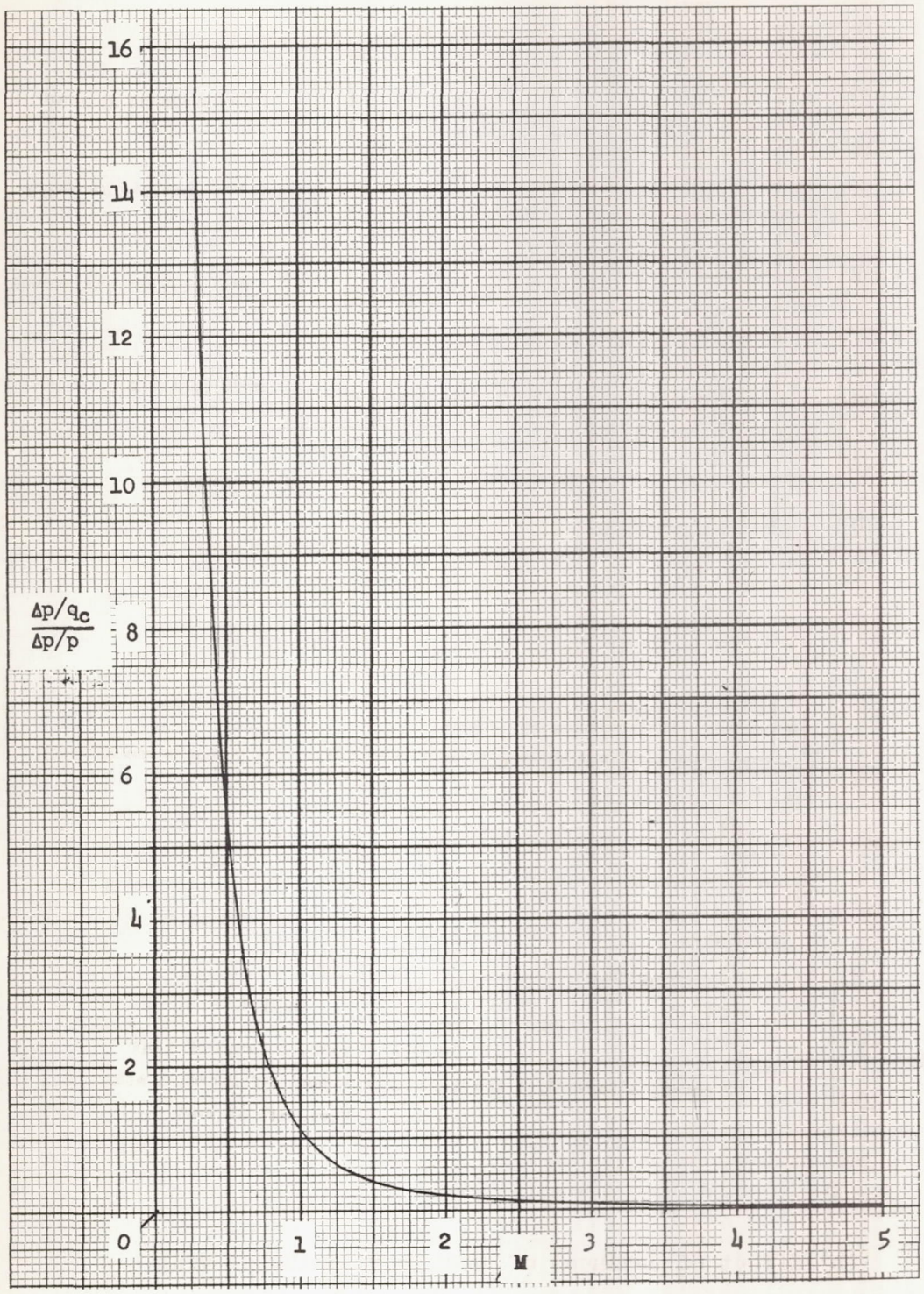


Figure 42.- Chart of converting $\Delta p/q_c$ to $\Delta p/p$ (based on calculations in ref. 40).

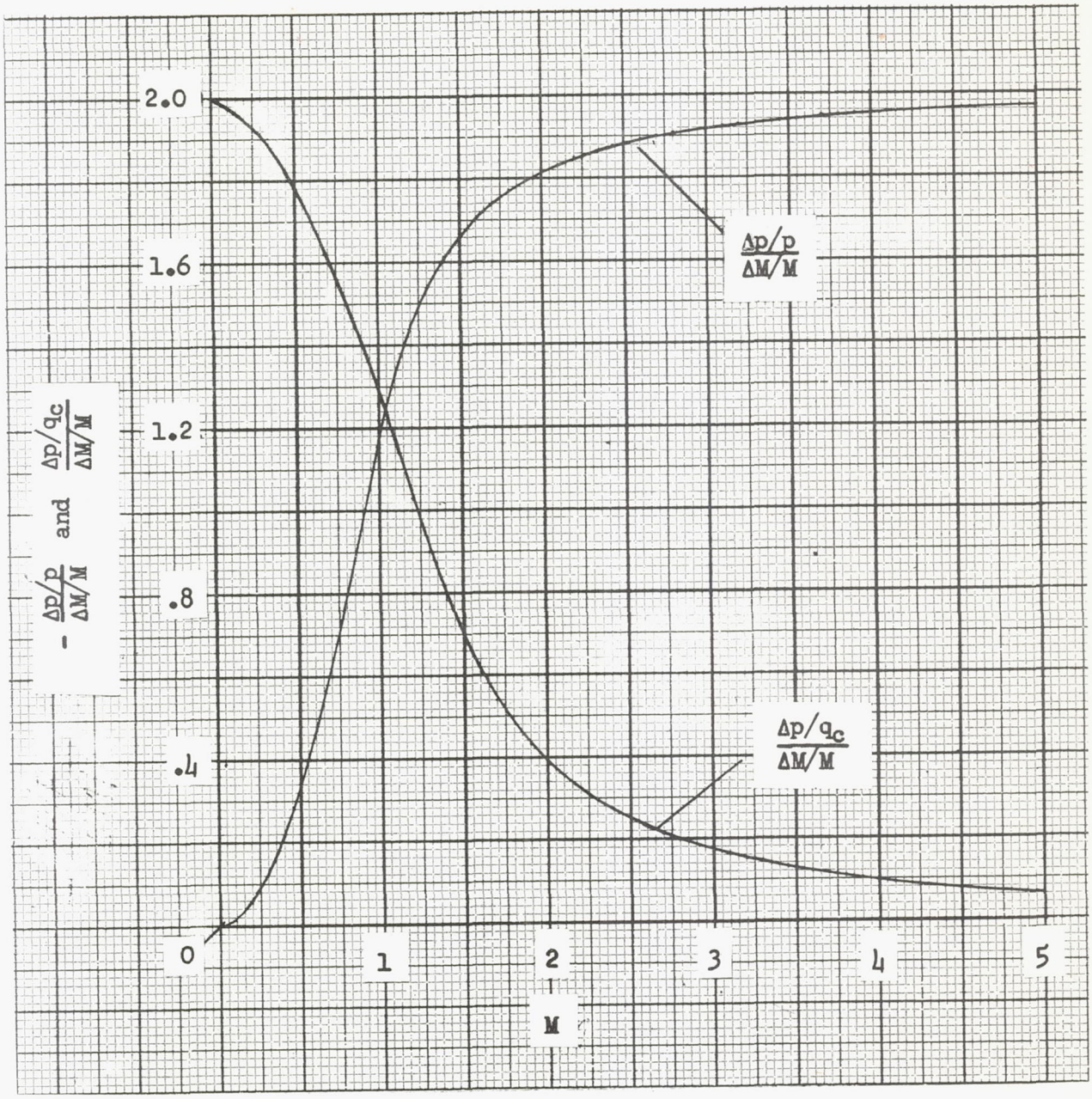


Figure 43.- Chart for converting $\Delta p/q_c$ or $\Delta p/p$ to $\Delta M/M$. At $M > 1$ the value of $q_c$ includes loss through normal shock (ref. 40).